SKI Report 2004:46

Research

# Near-Field Mechanical Analysis of Radioactive Waste Canister in Deep Repository

Sadek Baker
Ola Cliffordson
Göran Sällfors

December 2004

ISSN 1104–1374
ISRN SKI-R-04/46-SE

SKI

# SKI perspective

## Background

In the planned repository for spent nuclear fuel in Sweden according to the KBS-3 concept, a canister consisting of an outer copper shell and an cast iron insert plays a critical role in isolating the waste. The function of the copper shell is to provide the necessary corrosion resistance, while the cast iron insert provides the mechanical strength. The function of the bentonite is to provide a stable environment for the canister.

In general studies of the behaviour of the canister and the buffer material shall account for mechanical, hydraulic, thermal and chemical effects. In this study, near field mechanical behaviour is investigated.

## Purpose of the project

The purpose of the project is to investigate the mechanical behaviour of the canister while exposed to different mechanical loads. The loads investigated are uneven swelling of the bentonite (gives different loads on different parts of the canister) and shear movements in the rock. The analyses are performed with three-dimensional finite element methods, and different material models are used.

## Results

The analyses of uneven swelling of the bentonite did not give any plastic strains in the canister. Local swelling is therefore not a threat against the canister.

The results from the analyses of movements in the bedrock show that, as a consequence of large deviatoric stresses, plastic strains appear locally in the canister. However, the material properties for the materials in the canister show that the size of the deviatoric stresses is less than half of the failure stress. Thus, there seems to be no risk for local or total failure of the canister in case of movements in the bedrock.

## Effects on SKI work

This work will be used in the SKI evaluation of the SKB work on canister integrity. The report will also be used as one basis in SKI's forthcoming reviews of SKB's RD&D programme.

## Project information

Responsible for the project at SKI has been Fritz Kautsky.
SKI reference: 14.9-011239/01263

SKI Report 2004:46

Research

# Near-Field Mechanical Analysis of Radioactive Waste Canister in Deep Repository

Sadek Baker
Ola Cliffordson
Göran Sällfors

Geotechnical Engineering
Chalmers University of Technology
SE-412 96 Göteborg
Sweden

December 2004

# CONTENTS

# Abstract

The spent nuclear fuel and the radioactive materials formed during the operation of the Swedish nuclear power plants will be enclosed into tight metal canisters. These canisters will then be placed in large disposal boreholes drilled into the floor of the repository tunnels. Bentonite blocks will be placed to fill the space between the canisters and the boreholes. The main purpose with the bentonite is to provide a hydrological barrier.

In general the types of analysis required to study the behavior of the canister and the buffer material shall account for mechanical, hydraulic, thermal and chemical effects. In this study, only near field mechanical behavior is investigated.

Preliminary analyses are made based on simplified assumptions and on some simple two-dimensional finite element solutions. As a results of the preliminary analysis, limited tectonical movements in the bedrock and unfavorable local swelling are studied and modeled by the finite element code ABAQUS using tree-dimensional models.

The bentonite is modeled using two different material models, Mohr-Coulomb and Drucker-Prager, while the canister materials are modeled using a Drucker-Prager material model.

A certain form of sensitivity analysis for parameters has also been carried out.

The analyses of uneven swelling of the bentonite did not give any plastic strains in the canister. Local swelling is therefore not a threat against the canister. This load case is not the critical one.

The results from the analyses of movements in the bedrock show that, as a consequence of large deviatoric stresses, plastic strains appear locally in the canister. However, the material properties for the materials in the canister show that the size of the deviatoric stresses is less than half on the failure stress. Thus, there seems to be no risk for local or total failure of the canister in case of movements in the bedrock.

The conclusion from the finite element analyses is that the design of the nuclear waste canister (KBS-3) is sufficient to protect the nuclear waste from mechanical load.

# Sammanfattning

## Bakgrund

Vid driften av de svenska kärnkraftverken bildas radioaktiva restprodukter och avfall i form av bland annat använt kärnbränsle. Detta tas om hand och kommer enligt nuvarande planer att slutförvaras 500 meter ner i berggrunden inneslutet i täta kopparkapslar (KBS-3). Omkring kapslarna planeras ett skyddande buffertmaterial i form av bentonitlera.

Arbete pågår med att utforma och dimensionera anläggningen där slutförvaring skall ske. Slutförvaringen utformas för att skydda kapslarna mot yttre faktorer som kan tänkas påverka kapslarnas funktion, t.ex. rörelse i berget, jordbävning, korrosion, sättning, svällning etc.

Syftet med detta projekt har varit att studera hur olika mekaniska faktorer påverkar kapslarna och huruvida denna påverkan är av sådan omfattning att kapslarnas integritet hotas.

## Förenklade analyser

Inledningsvis gjordes förenklade analyser baserade på antaganden som medför resultat på säkra sidan. De fall som studerades var vertikala rörelser hos kapseln, spänningar i kapseln orsakade av svälltryck från bentoniten samt inverkan av eventuell tektonisk rörelse. Därvid framkom att eventuella vertikala rörelser hos kapseln orsakade av konsolidering, krypning eller bristande bärförmåga hos bentoniten inte i något avseende menligt kan påverka kapseln. De tryck som kan uppkomma som en följd av svällning hos bentoniten kan inte heller resultera i rörelser av sådan omfattning att kapseln kan förväntas komma i kontakt med det omgivande berget. Däremot visade de inledande beräkningarna att ogynnsamt geometriskt lokaliserad svällning skulle kunna medföra att viss flytning skulle kunna uppkomma i någon del av kapseln. Detsamma gällde effekterna av en tektoniskt betingad rörelse.

## Detaljerade analyser

Utifrån dessa analyser med förenklade modeller valdes därför att noggrannare analysera två olika mekaniska yttre belastningar. Den ena var böjning av kapseln till följd av förskjutning av ett sprickplan i berget i höjd med kapseln, och den andra var effekten av lokal ojämn svällning av buffertmaterialet kring kapseln. Analyser utfördes med finita elementprogrammet ABAQUS/Standard 5.7, där en tredimensionell solidmodell skapades, se Fig. I.

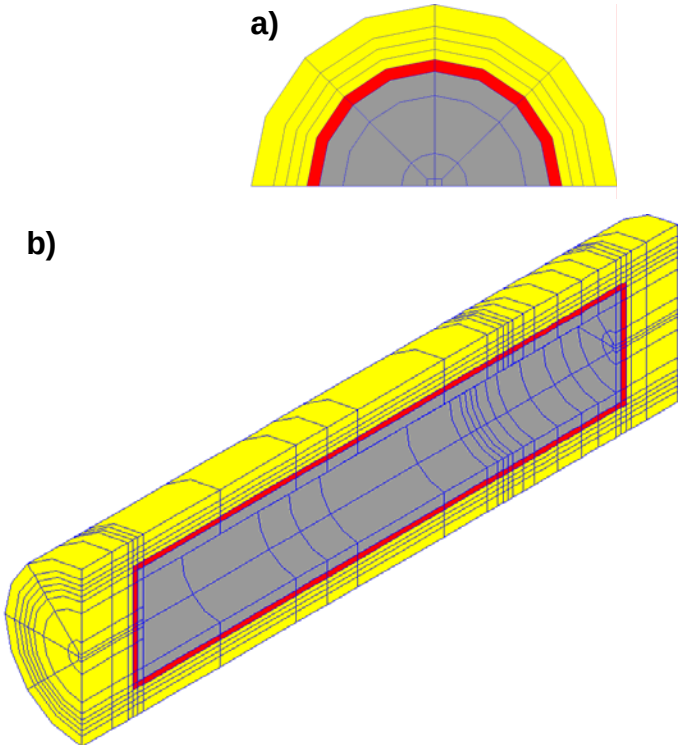


*Fig. I . Elementindelning för den 3-dimensionella modellen: a) sektion, b) 3-dimensionell vy*

## Materialmodeller

Vid analyserna har bentoniten modellerats med två olika materialmodeller utifrån kända materialegenskaper. Materialmodellerna var Mohr-Coulomb och Drucker-Prager. Valet av materialmodell för bentoniten påverkade i princip inte responsen och spänningssituationen för kapseln. De i kapseln ingående materialen modellerades som linjärelastoplastiska material med tillhörande E-moduler och flytfunktioner.

## Randvillkor

Randvillkoren som använts i analyserna visas i fig. II.

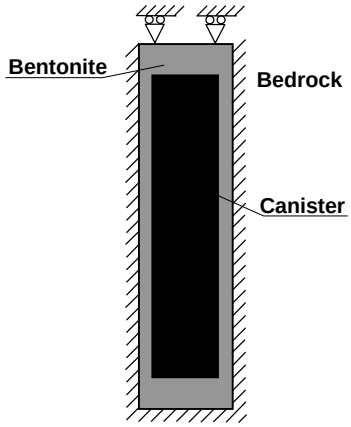


*Fig. II. Randvillkor*

## Ytterligare förenklingar

Följande förenklande antaganden har gjorts:

- Kapselns gjutna stålkärna har vid analyserna ersatts med en ekvivalent cylinderformad stålkärna med samma tröghetsmoment som den riktiga. Detta innebär att modellen innehåller färre element, vilket resulterar i kortare beräkningstider.
- I kontakten mellan bentonit och berg har friktionen antagits vara oändligt stor vilket innebär att bentonit och berg har full samverkan med varandra.
- All bentonit antas efter grundvattentillförsel bli fullständigt vattenmättad vilket ger upphov till en homogen svällning i hela modellen.
- Bentonitens olika svällningsstadier modelleras inte med undantag för ojämn svällning. De resulterande effekterna från svällningen i form av spänningar, portryck och portal anges istället som initialvillkor för analysen. Då det vid analyser visat sig att inga plastiska deformationer uppstår till följd av svällningen är detta en befogad förenkling som ger samma effekt på kapseln.
- Egenvikten hos kapsel och bentonit försummas i analysen då det ger ett försumbart bidrag till modellen jämfört med spänningarna som uppstår till följd av svällningen.
- Modellen har antagits vara helt odränerad vilket innebär att inget porvatten kan tillföras eller bortföras via ränderna. Analys av dränerad rand med konstant portryck (5000 kPa) har visat att det ger en försumbar skillnad jämfört med det odränerade fallet.

# Resultat och slutsatser

Analyserna av ojämn svällning av bentoniten kring kapseln gav inte plasticering i någon del av kapseln. Lokal svällning av bentoniten utgör således inte på något sätt ett hot mot kapselns integritet.

Mindre plastiska deformationer i kopparskalet och i stålet kan noteras vid den modellerade tektoniska rörelsen. Dessa är dock så pass små att kapselns existens inte äventyras. Detta visas tydligt ur materialens flytfunktion som beskriver dess deformationshårdnande, dvs den återstående hållfastheten i materialet då flytning börjat. Analyserna ger plastiska deformationer av storleksordningen 0,5-1% i kapseln.

Nedanstående diagram (fig. III) över flytfunktionen för stål och koppar visar att materialen vid dessa deformationer fortfarande befinner sig långt från brott.

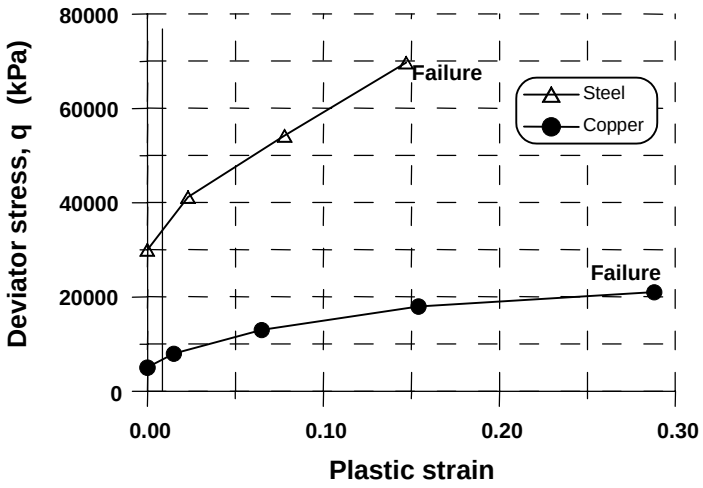


*Fig. III. Flytfunktion för koppar och stål.*

Bentonitens brottmodell påverkar inte responsen och spännings-situationen för kapseln. Den ger dock ett avvikande uppträdande hos bentoniten. Exempelvis påvisar Mohr-Coulombs brottmodell i detta fall större plasticering av bentoniten än Drucker-Pragers brottmodell. Tillförlitligheten hos denna analys är dock lite tveksam då värdet på bentonitens elasticitetsmodul kan avvika mycket från det experimentellt bestämda värdet.

Responsen från stålkärnan i den riktiga kapseln kan förenklas och modelleras med en ekvivalent stålkärna i form av en cylinder med motsvarande styvhet som den riktiga. Denna ekvivalenta stålkärna ger en respons hos kapseln som överenstämmer mycket väl med den riktiga stålkärnans.

Utifrån de utförda analyserna av kärnavfallskapseln KBS-3 kan dess mekaniska styrka anses vara fullgod för att skydda bränsleelementen från yttre mekaniska faktorer.

# 1 Introduction

The Swedish concept for storing spent nuclear fuel includes a number of barriers in order to insure that no radioactive material will leak into the surrounding soil or bedrock under of a period of almost 100,000 years. The radioactive material is enclosed in a canister, which is surrounded by bentonite, which shall prevent exchange of water with the surrounding bedrock. In order to insure this it is important that the canister remains intact, even if changes occur in the surrounding environment. Changes can be caused by a number of factors such as temperature, corrosion, chemical attack, tectonical movements or pressure differences due to unequal swelling of the surrounding bentonite.

The purpose with this project has been to gather sufficient information about the mechanical behavior and the stresses and strains, which will occur due to settlement, swelling and possible limited tectonical motions and their state whether they are of such dimension that they can jeopardize the integrity of the canister or not. In chapter 2 some results from simplified, preliminary analyses are presented. A number of different scenarios have been addressed and a few of them, where conservative assumptions indicated a need for further studies, were identified. As a result of the preliminary analysis uneven and unfavorable local swelling will be regarded and modeled in three-dimensional analyses. This also pertains to stresses caused by limited tectonical movements in the bedrock and how these will transform through the bentonite and affect the canister. To a certain extent the damaging and failure criteria for the canister have been studied.

A certain form of sensitivity analysis for the parameters at hand has also been carried out. All assumptions and conditions used in these calculations have been given in great detail.

# 2 Preliminary calculations for the integrity of the canister

## 2.1 Background

A number of scenarios that possibly could pose a threat to the canister has to be investigated. In this chapter results from a study where several different scenarios were addressed by performing preliminary calculations are presented. One purpose of the calculations was to identify the scenarios that needed further analysis. The investigation also resulted in identification of a number of scenarios that obviously, even with assumptions very much on the safe side, do not pose any threat what so ever to the canister.

The following scenarios were investigated:

1. Vertical settlement of the canister due to
   a) consolidation
   b) creep
   c) bearing capacity failure

2. Swelling of the bentonite
   a) vertical translation of the canister
   b) horizontal translation of the canister

3. Tectonic movement of the bedrock

Preliminary calculations have been made for the questions, given above. In some cases simple hand calculation methods have been used, while in other cases rather simple finite element methods were chosen. All calculations have been made with reasonable assumptions for the material parameters. Several supplementary calculations have been made with assumptions of the parameters which can be regarded as extreme values, in order to ensure that the scenario was harmless for the canister.

## 2.2 Vertical settlement of the canister

### 2.2.1 Consolidation settlement

The canister has been assumed to weigh 25 metric tons. The settlements will at the most be one or a few centimetres, even with the most conservative assumptions, and therefore the conclusion must be that neither the immediate settlement nor the consolidation settlement, pose any threat to the integrity of the canister.

### 2.2.2 Creep settlement

Values for the parameters which govern the creep behavior for the bentonite clay have not been available. Assumptions have therefore been made on the safe side by using values representative for much softer clays. The calculations point towards settlements which will be well below 10 cm, and neither in this case will the vertical settlement pose any threat to the canister. In these calculations it has been assumed that the safety against bearing capacity failure is sufficient, which is discussed in the following section.

### 2.2.3 Bearing capacity failure

Bearing capacity failure of the canister means that it due to its weight penetrates the bentonite and causes plastic yielding and transport of the bentonite material at its base. In these calculations perfect contact between the bentonite and the canister has been assumed. The theories for a point bearing pile have been used and thereby the calculations have been carried out for angles of internal frictions between 45 and 55 degrees. Any comparative undrained shear strength has not been found in the literature. The calculations, point towards the total factor of safety larger than 10 even for angles of internal friction as low as 35 degrees. It should be pointed out here that within geotechnical engineering a safety factor of approximately 3 is usually considered sufficient. An undrained analysis, with undrained shear strength for the bentonite should for a factor of safety of 3 require shear strength of approximately 80 kPa. This is a value, which is typical for stiff glacial clay and the bentonite shear strength is probably at least an order of magnitude larger. Thus bearing capacity failure is no threat what so ever for the canister.

## 2.3 Swelling of the bentonite

Bentonite is a swelling clay mineral and when bentonite gets in contact with water large swelling or movements occur. If swelling is restricted, large swelling pressures will develop instead.

### 2.3.1 Upward movement of the canister

For the case when water gets in contact with the bentonite at the bottom of the canister, it could result in a vertical lift-up of the canister. The swelling pressure will however diminish as the deformations develop and possible movement upwards would probably not exceed 10 centimetres. In order to make a somewhat better estimate, further knowledge about the swelling pressure of the bentonite is necessary compared to what has been available. More information about the material in the tunnel above is also needed.

### 2.3.2 Horizontal translation of the canister

For the case when water flows into the bentonite only on one side large local swelling can occur. These loads on the canister can in turn result in a translation of the canister or a bending loading. The risk occurring and which need to be investigated is whether the canister will be pushed over to the other side of the hole and get in contact with the bedrock, or if the bending loading of the canister is of such magnitude that the integrity of the canister can be jeopardized due to large bending movements or deformations. Furthermore the case with the local pressure against the canister must be investigated.

#### 2.3.2.1 Translation of the canister towards the bedrock

The problem is about the same as for the case of heave due to swelling at the bottom. Not even for this load case can any risk be considered at hand. It is thus most unlikely that the canister should get in contact with the bedrock on the other side.

#### 2.3.2.2 Local swelling resulting in bending

In the case when the swelling occurs along the canister it will be subjected to bending. This can also be simulated with calculations with different degrees of complexity. The calculations performed here have been made with a finite element programme, but a number of simplifications have been necessary to make in order to handle the calculations. The conclusions are briefly given below and finally the results are discussed.

***Assumptions and limitations of the results from the study performed***

The first assumption is that the geometry is considered as two-dimensional, where the three-dimensional effects are neglected. This can for certain cases be favourable and in other cases unfavourable assumptions. The constitutive models that are used have all been linear elastic and no yield stresses have been simulated. For simplicity the weight of the canister and the bentonite has been neglected. The stiffness of the canister has been simulated with a beam element, which has a given stiffness, but which in principle does not have any thickness. Comparative calculations, where the canister is modeled in the same way as for soil elements to simulate the actual dimension of the canister, show that the strain and deformations will be of the same order of magnitude, which in turn indicate that this simplification of the canister by modeling it with beam elements seem to be reasonable. Concerning the swelling pressures calculations have been carried out for two levels, 5 MPa and 40 MPa. It shall be pointed out that the calculations have not simulated an inner swelling pressure but instead the swelling pressure has been brought about as a corresponding pressure. Thereby the bentonite gets compression on the pressure side instead of an expansion, but for the canister and the bentonite on the other side of the canister this is of minor importance. In this preliminary calculation the canister has been considered as a homogeneous iron cylinder and has been modeled as a beam element and the calculation described the rest of the chapters modeling was made with ordinary elements. Certain deficiencies can occur in the calculations when the difference in stiffness between two adjacent elements becomes too large. That is the reason for also testing the beam element.

***Results from Calculations***

The calculations show that the most severe loading case is when a relatively local but strong swelling occurs adjacent to the end and on one side of the canister. This should with the simplified assumptions that were made here lead to bending moments in the canister of such magnitude that yield may occur in the canister. The assumption of a solid canister does result in a larger bending stiffness but this will only affect the bending moments to a small degree.

## 2.4 Tectonic movement of the bedrock

In a longer time perspective the bedrock could deform along an unfavourably situated crack. Calculations have been made with a case of distortion of the bedrock of such an unfavourably localised crack.

***Assumptions***

The assumptions are the same as for the previous loading cases. A deformation is modeled as a 10-centimeter-parallel distortion of the bedrock. Three different locations of a single crack have been analysed.

***Results of calculations***

The calculations in this case lead to, with the assumptions made, that the bending moments in the canister will become of such order of magnitude that they under certain circumstances might result in yielding in parts of the canister.

# 3 Models for material

## 3.1 Modeling

In order to model the future repository of spent nuclear fuel a few simplifying assumptions are necessary to make. This concerns the geometry, the properties of the different materials and the interaction between them.

Initially the geometry is modeled as a stick model, which in this case is rotational symmetric with sizes according to the figures given later on. The true geometry would probably only marginally deviate from the assumed, and then mostly depending on minor imperfections due to manufacturing errors. However, in this project the overlying tunnel with its bentonite is not modeled.

In this model the surrounding bedrock will be modeled as well as the bentonite and the canister. The properties of these materials are described with a few well-established models, which are briefly described below.

The mathematical modeling is then performed in a FEM-method in the program ABAQUS. Great care was taken to model the material in such a way that the results from the analysis will be as reliable as possible, still not being too complicated.

### 3.1.1 Bedrock

The bedrock is in comparision with bentonite very stiff and of extremely good quality. As it is the local effects on the canister, which are of greatest interest, the bedrock is assumed to be indefinitely stiff and will only enter into the calculations as a boundary condition.

### 3.1.2 Canister

The canister is manufactured from iron and copper. The materials are linear elastic and the parameters used in this calculation are $E$ and $\nu$. Iron as well as copper yields when the stresses become high enough and this is modeled by the Drucker-Prager yield criterion, which is treated more in detail below.

### 3.1.3 Bentonite

Bentonite is a swelling clay mineral and its strength and deformation properties are among other things depending on the state of stress, stress history, density, water content and temperature. An accurate modeling of these properties requires very complicated models with a large number of parameters describing the properties. Models, requiring more than 30 parameters to describe the property of the material, have been found in the literature. This task mainly concerns whether the integrity of the canister is jeopardized by possible tectonical movements in the bedrock or by pressure differences, which could be caused by an unequal swelling of the bentonite. It does not include the effect of temperature or the transient part of diffusion of water or flow of water. Modeling thus is a static case of loading with no temperature effects. In this

situation the bentonite can be modeled with good accuracy with the Durcker-Prager yield hypothesis or with the so-called Cam-Clay model.

## 3.2 Drucker-Prager

The yield criterion by Drucker-Prager is a simplification of Mohr-Coulomb's yield criterion and is based on von Mises yield hypothesis. The von Mises yield criterion does account as Drucker-Prager for all three main principal stresses. During the numerical calculations (FEM-analysis) Mohr-Coulomb's yield criterion can cause numerical difficulties as the yield criterion in the π-plane is complicated and has the shape of a hexagon. It is the corners in the hexagon, which cause the numerical difficulties. In order to avoid these problems Drucker-Prager's yield criterion (Drucker and Prager, 1952) introduce a smooth circular surface in the π-plane with no corners describing the yield area with elasto-plastic finite element analysis (Figure 3.1). The yield criterion is in the shape of a cone in the principal stress space.

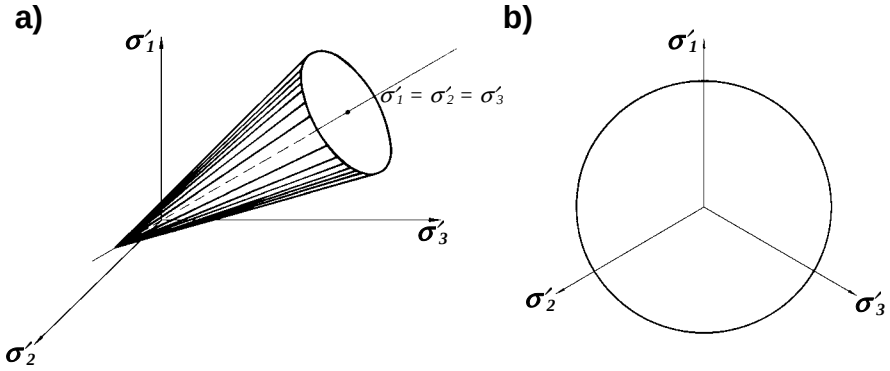


***Figure 3.1*** *Drucker-Prager's yield criterion: a) principal stress space, b) on the π-plane (Chen and Mizuno, 1990).*

The yield criterion is described as a function of the deviator stress ($q$) and the mean effective stress ($p'$) together with the two material parameters $\beta$ and $d$, equation (3-1), according to Fang, (1991). For the special case where $\beta$ is equal to zero the Drucker-Prager yield criterion is identical to von Mises hypothesis of deviator work.

$$q = d + B \cdot p' \tag{3-1}$$

where

$$B = \tan\beta \tag{3-2}$$

$$p = \frac{\sigma'_1 + \sigma'_2 + \sigma'_3}{3} \tag{3-3}$$

$$q = \sigma'_1 - \sigma'_3 \tag{3-4}$$

The material parameters $\beta$ and $d$, can be compared with Mohr-Coulomb's parameters $\phi'$ and $c'$. The Drucker-Prager yield criterion in the $pq$-plane is given in equation (3-1) and is shown in Figure 3.2.

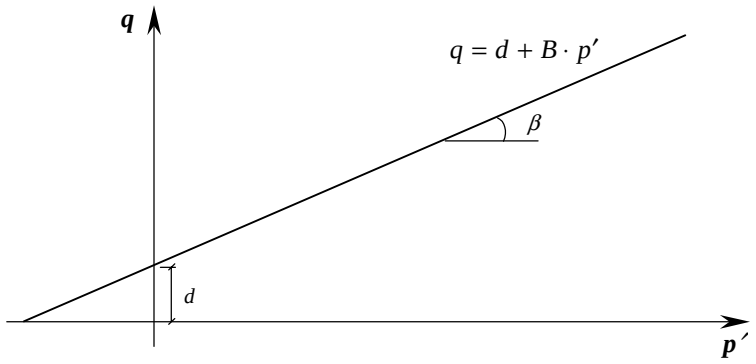


***Figure 3.2.*** *Drucker-Prager yield criterion in the pq-plane (Fang, 1991).*

The material parameters $\beta$ and $d$ in the Drucker-Prager model can be derived and expressed in the more commonly used Mohr-Coulomb parameters $c'$ and $\phi'$.

When deriving $\beta$ and $d$ it is customary to start with the $pq$-plane (Figure 3.2). The Y-axis in the diagram can be written as

$$Y_{DP} = q = \sigma_1' - \sigma_3' \tag{3-5}$$

and the X-axis

$$X_{DP} = p = \frac{\sigma_1' + \sigma_2' + \sigma_3'}{3} \tag{3-6}$$

When considering the three-dimensional case, i.e. $\sigma'_2 = \sigma'_3$ and $\sigma'_1 > \sigma'_3$, the following equations for the coordinate axes are obtained

$$Y_{DP} = \sigma_1' - \sigma_3' \tag{3-7}$$

$$X_{DP} = \frac{\sigma_1' + 2\sigma_3'}{3} \tag{3-8}$$

The transformation equations for the Cartesian coordinate system ($X$, $Y$, $Z$) and the coordinate system for principal stresses ($\sigma'_1$, $\sigma'_2$, $\sigma'_3$) in the $\pi$-plane is, according to Chen and Mizuno, 1990:

$$\begin{bmatrix} \sigma_1' \\ \sigma_2' \\ \sigma_3' \end{bmatrix} = \begin{bmatrix} 0 & \frac{2}{\sqrt{6}} & \frac{1}{\sqrt{3}} \\ -\frac{1}{\sqrt{2}} & -\frac{1}{\sqrt{6}} & \frac{1}{\sqrt{3}} \\ \frac{1}{\sqrt{2}} & -\frac{1}{\sqrt{6}} & \frac{1}{\sqrt{3}} \end{bmatrix} \begin{bmatrix} X \\ Y \\ Z \end{bmatrix} \tag{3-9}$$

or

$$\begin{bmatrix} X \\ Y \\ Z \end{bmatrix} = \begin{bmatrix} 0 & -\frac{1}{\sqrt{2}} & \frac{1}{\sqrt{2}} \\ \frac{2}{\sqrt{6}} & -\frac{1}{\sqrt{6}} & -\frac{1}{\sqrt{6}} \\ \frac{1}{\sqrt{3}} & \frac{1}{\sqrt{3}} & \frac{1}{\sqrt{3}} \end{bmatrix} \begin{bmatrix} \sigma_1' \\ \sigma_2' \\ \sigma_3' \end{bmatrix} \tag{3-10}$$

The Y-axis for the Mohr-Coulomb's yield criteria in the π-plane can according to equation (3-10) be written as:

$$Y_{MC} = \tfrac{2}{\sqrt{6}}\sigma_1' - \tfrac{1}{\sqrt{6}}\sigma_2' - \tfrac{1}{\sqrt{6}}\sigma_3' \qquad (3\text{-}11)$$

When three-dimensional stresses are accounted for the following expression is obtained:

$$Y_{MC} = \tfrac{2}{\sqrt{6}}\left(\sigma_1' - \sigma_3'\right) \qquad (3\text{-}12)$$

Mohr-Coulomb's yield criterion in *X*- and *Y*- direction on the π-plane during three-dimensional stress is:

$$Y_{MC} = \frac{\sqrt{3}\left(1+\sin\phi'\right)}{3-\sin\phi'} X_{MC} + \frac{2\sqrt{6}c'\cdot\cos\phi'}{3-\sin\phi'} \qquad (3\text{-}13)$$

For $X_{MC} = 0$ the following is obtained

$$Y_{MC} = \frac{2\sqrt{6}c'\cdot\cos\phi'}{3-\sin\phi'} \qquad (3\text{-}14)$$

and for $X_{DP} = 0$ one obtains according to Figure 3.2

$$Y_{DP} = d \qquad (3\text{-}15)$$

The interaction between Mohr-Coulomb and Drucker-Prager in the *Y*-direction on the π-plane for $X = 0$ will be

$$\frac{Y_{MC}}{Y_{DP}} = \frac{\tfrac{2}{\sqrt{6}}\left(\sigma_1' - \sigma_3'\right)}{\left(\sigma_1' - \sigma_3'\right)} = \frac{\left(\dfrac{2\sqrt{6}c'\cdot\cos\phi'}{3-\sin\phi'}\right)}{d} \qquad \Rightarrow$$

$$d = \frac{\sqrt{6}}{2}\cdot\frac{2\sqrt{6}c'\cdot\cos\phi'}{\left(3-\sin\phi'\right)} \qquad \Rightarrow$$

$$d = \frac{6c'\cdot\cos\phi'}{3-\sin\phi'} \qquad (3\text{-}16)$$

Equation (3-16) shows the mathematical equation for *d* and the Mohr-Coulomb parameters $c'$ and $\phi'$ for three-dimensional stresses.

To express the relation between $\beta$ and $\phi'$ equation (3-1) can be written as

$$\sigma_1' - \sigma_3' = d + B\cdot\left(\frac{\sigma_1' - 2\sigma_3'}{3}\right) \qquad (3\text{-}17)$$

Rewriting of the above equation using the principal stresses $\sigma'_1$ and $\sigma'_3$ in a Cartesian coordinate system on the π-plane will yield

$$\frac{2}{\sqrt{6}}Y_{MC} - \frac{X_{MC}}{\sqrt{2}} + \frac{Y_{MC}}{\sqrt{6}} = d + \frac{B}{3}\left(\frac{2}{\sqrt{6}}Y_{MC} + \frac{2}{\sqrt{2}}X_{MC} - \frac{2}{\sqrt{6}}Y_{MC}\right)$$

which can be simplified to

$$\frac{3}{\sqrt{6}}Y_{MC} - \frac{X_{MC}}{\sqrt{2}} = d + \frac{B}{3}\left(\frac{2}{\sqrt{2}}X_{MC}\right) \qquad (3\text{-}18)$$

When $Y_{MC} = 0$, $X_{MC}$ is obtained according to equation (3-13) as

$$X_{MC} = -\frac{2\sqrt{2}c' \cdot \cos\phi'}{\left(1+\sin\phi'\right)} \qquad (3\text{-}19)$$

Equation (2-16) and (2-19) will give substituted into equation (3-18):

$$\frac{2c' \cdot \cos\phi'}{1+\sin\phi'} = \frac{6c' \cdot \cos\phi'}{3-\sin\phi'} - \frac{B}{3} \cdot \left(\frac{4c' \cdot \cos\phi'}{1+\sin\phi'}\right) \quad \Rightarrow$$

$$B = \frac{6 \cdot sin\phi'}{3-\sin\phi'} \qquad (3\text{-}20)$$

where $B = \tan\beta$.

In the same manner the dependence of $\beta$ and $d$ and the Mohr-Coulomb parameters $c'$ and $\phi'$ can be derived for triaxial tension and plane strain. Table 3.1 shows the derived equations for Drucker-Prager and the Mohr-Coulomb parameters according to Chen and Mizuno, 1990.

***Table 3.1*** *The relation between Drucker-Prager and Mohr-Coulomb parameters (Chen and Mizuno, 1990).*

| **Boundary conditions** | **tan$\beta$** | ***D*** |
|---|---|---|
| Triaxial compression | $\frac{6 \cdot \sin\phi'}{\left(3-\sin\phi'\right)}$ | $\frac{6c' \cdot \cos\phi'}{\left(3-\sin\phi'\right)}$ |
| Triaxial tension | $\frac{6 \cdot \sin\phi'}{\left(3+\sin\phi'\right)}$ | $\frac{6c' \cdot \cos\phi'}{\left(3+\sin\phi'\right)}$ |
| Plane strain | $\frac{6 \cdot \sin\phi'}{\sqrt{3+4 \cdot \tan^2\phi'}}$ | $\frac{6c' \cdot \cos\phi'}{\sqrt{3+4 \cdot \tan^2\phi'}}$ |

The comparison between the Mohr-Coulomb and Drucker-Prager yield criterion in the *pq*-plane and in the π-plane is given in Figure 3.3. Drucker-Prager yield criterion can not be defined for tension and compression simultaneously. During comparison two circles are therefore needed for the Drucker-Prager yield criteria.

The shape of the yield surface is defined according to the equation in the *pq*-plane below

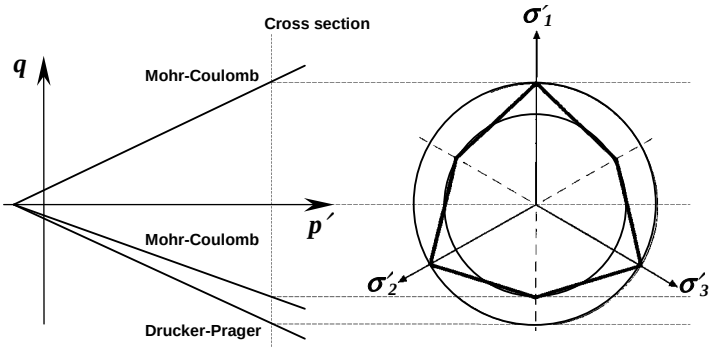


***Figure 3.3*** *Mohr-Coulomb and Drucker-Prager's yield criterion in the pq-plane and in the π-plane (Vermeer, 1995).*

# 3.3 Cam-Clay model

Roscoe et al, (1963), at Cambridge University presented an elasto-plastic model for how the yield surface in soils can be defined regarding deviator stresses ($q$) and mean effective stresses ($p'$). Depending on different soil material behaviour the model seperated between frictional material (*Granta Gravel* model) and clay (*Cam-Clay* model). The models are in principle identical. The difference is that the Granta-Gravel model does not account for elastic strain for stresses below the preconsolidation pressure. The clay in Cam-Clay model is assumed to swell and compress elastically during off- and onloading in this stress area (Figure 3.4).

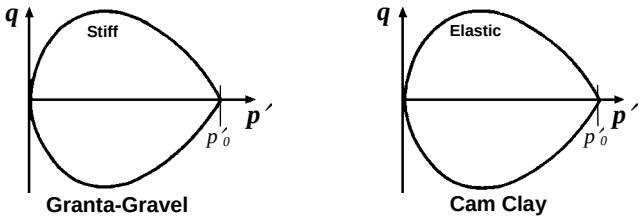


***Figure 3.4*** *Yield surface for Granta Gravel and Cam-Clay models (Schofield and Wroth, 1968).*

The preconsolidation of the material is assumed to result in an elastic stress state bounded by a yield surface. Within this surface all deformations are assumed to be elastic. If the stress state results in an overriding of the yield surface plastic deformations occur, which in turn results in large volumetric changes, changed preconsolidation stresses and corresponding changes in the state boundary surface.

In the model the soil is assumed to be idealelastic-plastic material with no anisotropy, i.e. isotropic material. If the soil is sheared continuously until deformation continues without any changes in volume and that the shear stresses are increased then the soil has reached its *Critical state* period. In this state the deviator stress is a direct function of the mean effective stress, $q = Mp'$.

The shape of the yield surface is defined according to the equation in the *pq*-plane below

$$q + Mp' \cdot \ln \frac{p'}{p'_0} = 0 \qquad (3\text{-}21)$$

When a material is exposed to isotropic stress, $\sigma'_1 = \sigma'_2 = \sigma'_3$, it is not exposed to any shear stresses, i.e. $q = 0$. The effect of an increasing isotropic pressure is an increase of the consolidation stresses for the material. The consolidation stress results in a decrease in volume of the material with a permanent reduction of pores, i.e. the specific volume of the material decreases. The decrease in volume of the material in combination with the yield surface in the *pq*-plane gives a three-dimensional yield surface in the *pqV*-system (Figure 3.5) where *V* denotes the specific volume.

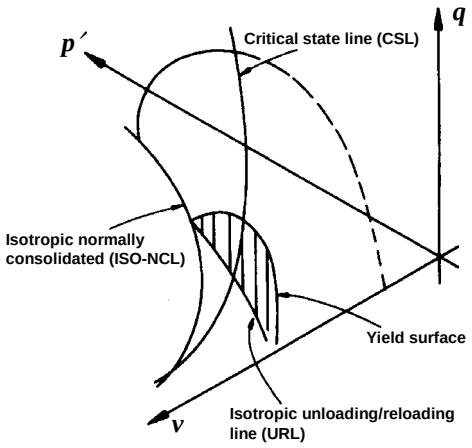


***Figure 3.5*** *Three-dimensional yield surface and "critical state line" in the pqV-system (Powrie, 1997).*

Figure 3.6 shows the shape of the yield surface or the state boundary surface in the three-dimensional projection on the *pq*-plane and on the *pV*-plane. In the Cam-Clay model the volume of the material is assumed to be a linear function of the natural logarithm of the mean effective stress (ln *p´*), which is shown by the isotropic normal consolidation curve (ISO-NCL) in Figure 3.6.

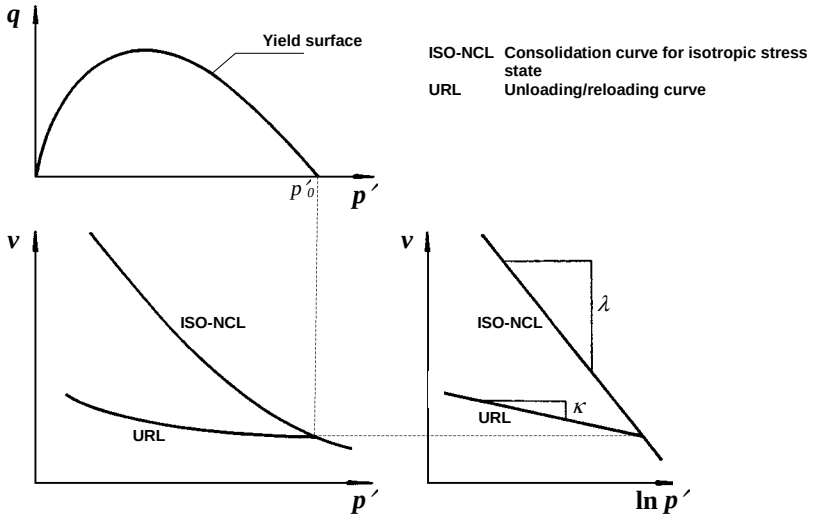


***Figure 3.6*** *Yield surface and compression properties for the Cam-Clay model (Schofield and Wroth, 1968).*

During isotropic consolidation the following linear equation for the specific volume is valid, according to Figure 3.6:

$$v = N - \lambda \cdot \ln p' \qquad (3\text{-}22)$$

During unloading plastic deformation will remain and the elastic deformation bounces back, which results in an increase of the specific volume along the unloading curve (URL unloading-reloading-line) see Figure 3.6. The specific change of volume of the material (swelling) during unloading is defined as:

$$v = v_\kappa - \kappa \cdot \ln p' \qquad (3\text{-}23)$$

When the material is reloaded the change of volume follows the elastic part of the curve until it reaches the normal consolidated line (ISO-NCL) and plastic deformations start to develop again.

The material parameter $\lambda$ can be seen as an inverted compression number for the bulk modulus and $\kappa$ for the corresponding swelling index. The parameter $\lambda$ contains plastic as well as elastic deformations and the pure plastic part constitutes the difference ($\lambda$-$\kappa$).

The original Cam-Clay models have been modified to a model which also is valid for non-cohesive soil, so called *modified Cam-Clay* according to Roscoe and Burland, (1968). This is the model which today normally is used for numerical calculations. In the modified Cam-Clay model the yield surface has the shape of an ellipse in the *pq*-plane with the equation

$$\frac{p'}{p'_0} = \frac{M^2}{\left(M^2 + \eta^2\right)} \qquad (3\text{-}24)$$

where $\eta = \frac{q}{p'}$ , which gives

$$q^2 + M^2 p'^2 = M^2 p'_0 p' \qquad (3\text{-}25)$$

The original Cam-Clay model was defined as a logarithmic spiral, which mathematically is easier to handle than an ellipse.

The interrelation between the yield surface and compression characteristics for modified Cam-Clay is given in the following figure.

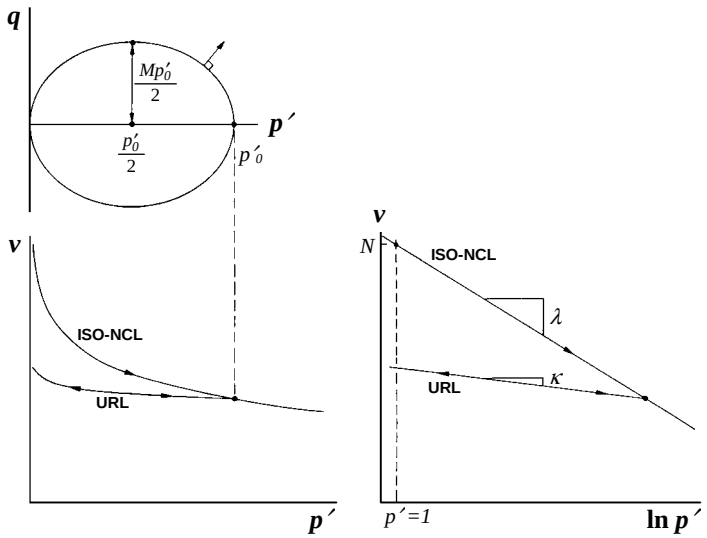


***Figure 3.7*** *Elliptic yield surface and compression characteristics in the modified Cam-Clay model (Wood, 1990).*

The Cam-Clay model is an important contribution to modern soil mechanics where it is very applicable and comparatively easy to use. The model has as all models certain shortcomings. It can for example not distinguish between one-dimensional and isotropic stress, and the shape of the yield surface has little resemblance to those which are obtained from laboratory tests on certain natural soils, according to Wood, (1990). No simple model in the *pq*-plane can however be completely general and valid for all types of load changes and stress paths. For a better modeling of true soils a much more complicated model is necessary as for example a model that has been developed at MIT, MIT-EC3 (Wittle and Kavvadas, 1994).

The term *Critical state strength* is important in this discussion. Critical state describes the state in the soil when it has reached a constant volume after substantial deformations. The material which earlier either dilated or contracted during shear will continue to plastically shear with no change in volume, deviator stress or mean effective stress, i.e. *q*, *p´* and *q*, *p´* are constant. This plastic state is called critical state and is defined, according to Wood, (1990), as

$$\frac{\partial p'}{\partial \varepsilon_s} = \frac{\partial q}{\partial \varepsilon_s} = \frac{\partial \varepsilon_v}{\partial \varepsilon_s} = 0 \qquad (3\text{-}26)$$

where $\varepsilon_v = \varepsilon_1 + \varepsilon_2 + \varepsilon_3$

$\varepsilon_s = \frac{2}{3}\left(\varepsilon_1 - \varepsilon_3\right)$

The great advantage with Critical state as a definition of yield is that it is not affected by stress history, i.e. if the soil has been preconsolidated or not (loose or compact) has no influence on the results. Critical state is obtained when all cohesive forces in the material have ceased and the void ratio is constant. Therefore the original void ratio of the material is of no meaning.

Critical state is described in the *pq*-plane as a linear function, the so called *Critical state line* (CSL), which goes through the top value of the yield surface and is defined by the following equation

$$q = Mp' \qquad (3\text{-}27)$$

The yield surface of the soil and the critical state depends on $p'$, $q$ and $v$ and can be visualized as a three-dimensional surface, (Figure 3.8).

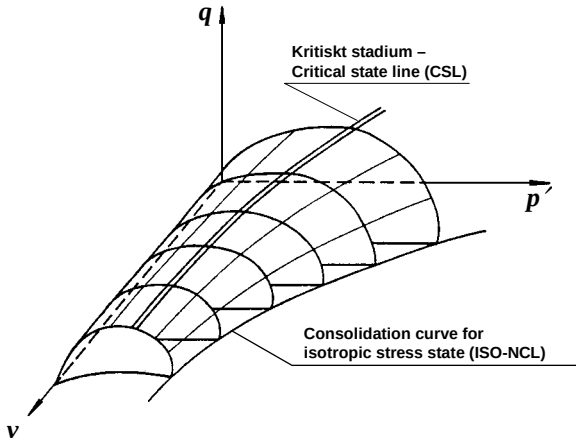


***Figure 3.8*** *Three-dimensional yield surface, elastic plane and the relation between stress path and change of volume (Wood, 1990).*

Projections on the three different planes are given in Figure 3.9.

The equation for the *Critical state* line on the ln($p'$)$v$-plane is

$$v_{cs} = \Gamma - \lambda \ln p_{cs} \qquad (3\text{-}28)$$

The part of the yield surface where deviator stresses are larger than the critical state on the *pq*-plane in Figure 3.9 indicates a dilative behavior during shear. This is valid for rather overconsolidated clay. When the stress reaches the yield surface within this area the soil will expand, while the correspondent preconsolidation pressure and yield surface will decrease and the material becomes strain softening. For deviator stresses below the critical stress large plastic deformations occur when the stress path reaches the yield surface, the corresponding preconsolidation pressure and yield surface increases and the material behaves as strain hardening.

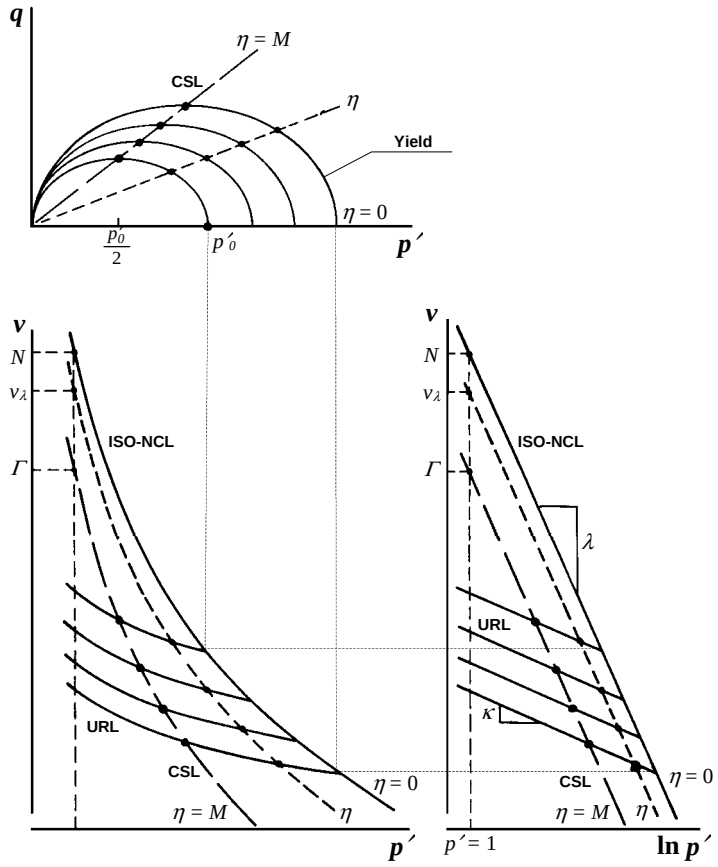


***Figure 3.9*** *Yield Surfaces and Critical state lines (CSL) on pq-, pv- and, ln(p)v-plane (Wood, 1990).*

The critical state parameter $M$ can be derived and expressed as a function of the internal fiction of the material $\phi'$. Critical state means that the cohesion in the soil is no more there, i.e. $c' = 0$. This criterion is introduced into the Mohr-Coulomb yield criterion, which yields

$$\sigma_1' - \sigma_3' = \sigma_1' \sin\phi' + \sigma_3' \sin\phi' \quad \Rightarrow$$

$$\sigma_1'(1 - \sin\phi') = \sigma_3'(1 + \sin\phi') \quad \Rightarrow$$

$$\frac{\sigma_3'}{\sigma_1'} = \frac{(1 - \sin\phi')}{(1 + \sin\phi')} \qquad (3\text{-}29)$$

The definition of the deviator stress, $q$, and the mean effective stress, $p'$, is for triaxial compression ($\sigma'_2 = \sigma'_3$)

$$q = \sqrt{\tfrac{1}{2}\left((\sigma_1' - \sigma_2')^2 + (\sigma_2' - \sigma_3')^2 + (\sigma_3' - \sigma_1')^2\right)} \qquad (3\text{-}30)$$

$$p = \frac{\sigma_1' + \sigma_2' + \sigma_3'}{3} = \frac{\sigma_1' + 2\sigma_3'}{3} \qquad (3\text{-}31)$$

By substituting equation (3-30) and (3-31) in the definition for *M* the following is obtained

$$M = \frac{q}{p'} = \frac{\sigma_1' - \sigma_3'}{\left(\frac{\sigma_1' + 2\sigma_3'}{3}\right)}$$

Which after simplification and introduction of equation (3-29) results in

$$M = \frac{6 \cdot \sin\phi'}{3 - \sin\phi'} \qquad (3\text{-}32)$$

The relation for material in tension is obtained in the same manner, according to Atkinson and Bransby (1978), as

$$M = \frac{6 \cdot \sin\phi'}{3 + \sin\phi'} \qquad (3\text{-}33)$$

Equation (3-32) and (3-33) is given in the *pq*-plane according to the figure below (Figure 3.10).

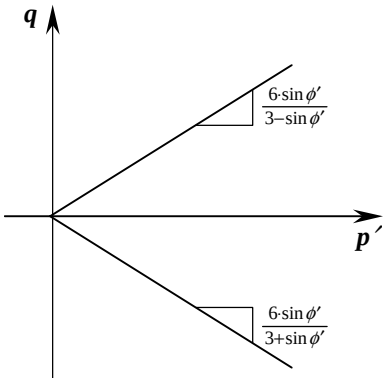


***Figure 3.10*** *Relation between the Critical state parameter, M, and the angle of internal friction, $\phi'$, (Wood, 1990).*

# 4 Modeling tools

## 4.1 General

Finite element analysis (FEM-analysis) of a problem using a computer program generally consists of the following steps (Samuelsson and Wiberg, 1995). The steps are:

1. Idealization of the problem, i.e. simplification and modeling of the problem. Boundary conditions are determined.
2. Discretization. The model is divided into elements.
3. Element analysis. The stiffness matrix for the elements, $S^e$ is evaluated for each of the elements.
4. Analysis. The elements are linked together and a system of equations is established for the whole model, which gives the solution to the problem.
5. Post-processing. The important parameters such as stress, strain etc are calculated and evaluated.
6. Evaluation. A simple evaluation and control to check that the results are reasonable is performed.

In order to model a problem in a satisfactory way it is important that the parameters used, e.g. geometry, boundary conditions, models for the material etc., are established in a correct way. As in many cases one has insufficient information about the corresponding material and its properties it is important to have this in mind when analysing the results. It is therefore recommendable to check the effect of a variation of the value for the parameters showing the largest amount of scatter.

## 4.2 Theory and methodology for solving the equations

The computer program used is ABAQUS. The method for solving the problem is different for non-linear problems, i.e. the best strain curve is modeled as a non-linear function, (Figure 4.1), and linear problems. When solving non-linear problems in ABAQUS the load is given as a function of fictive time. A calculation is divided into several load steps in which different loads, boundary conditions and procedure of analysis can be chosen. The load steps are in turn divided into time steps or so called time increments in order to closely follow the non-linear response of the material.

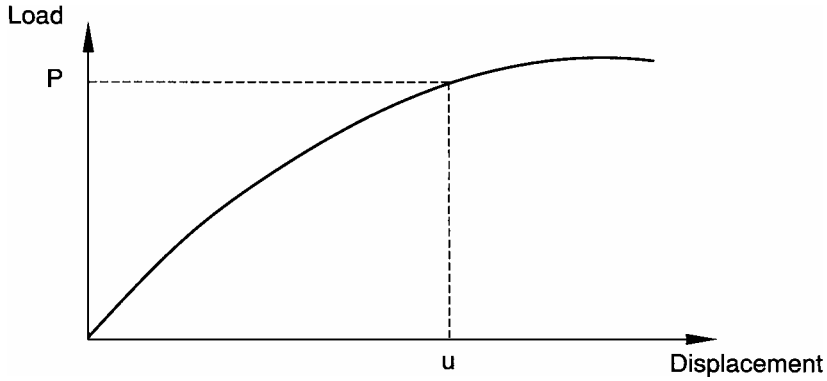


***Figure 4.1*** *Example of non-linear material properties (Hibbit et al, 1997).*

ABAQUS 5.7 uses Newton's method for iteration and reaches an approximate equilibrium for each time step. If the model is not in equilibrium after one iteration, the program ABAQUS uses a new iteration. For each iteration, which is completed the solution that ABAQUS has calculated shall go towards equilibrium (convergence). If this is not the case the process is said to divert. If the process diverts ABAQUS interrupts the process and starts over again with a smaller time increment.

The requirement for a free body to be in equilibrium is that the node forces, *I*, and the outer forces, *P*, are in balance, i.e.

$$P - I = 0 \qquad (4\text{-}1)$$

The origin of the internal node forces are stresses within the elements that the nodes belong to.

When ABAQUS is solving for equilibrium the program makes use of small load steps, $\Delta P$, together with the tangent stiffness of the total structure, $K_0$, (the tangent of the curve at a displacement $u_0$), in order to calculate the distortion correction, $c_a$. The first iteration is given in Figure 4.2.

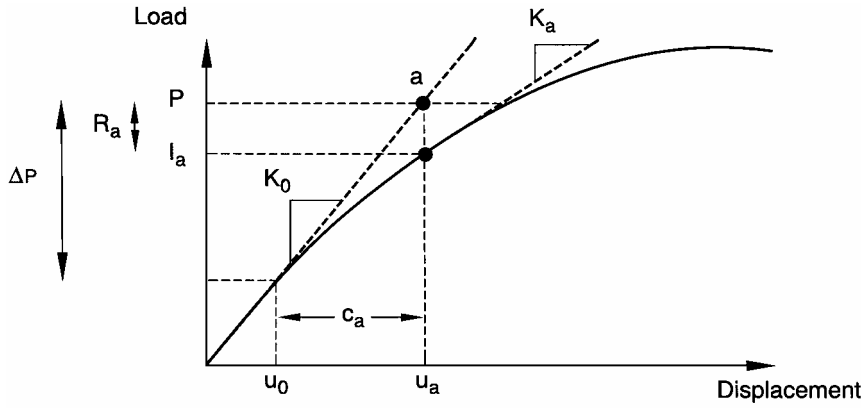


***Figure 4.2*** *The first iteration in one time increment (Hibbit et al, 1997).*

When the first iteration is completed ABAQUS compares the internal forces of the structure with the external applied forces and determines the force residual, *R*, for the iteration.

$$R_a = P - I_a \qquad (4\text{-}2)$$

If $R_a$ is zero in all degrees of freedom in the model the point *a* is on the stress strain curve of the structure and the structure is thus in equilibrium. For **non-linear** problems however, the residual, $R_a$, is never exactly zero. ABAQUS then compares the residual with the given tolerance. If the residual is less than the tolerance in all nodes ABAQUS checks that distortion correction, $c_a$, is small in comparison with the total distortion, $\Delta u_a = u_a - u$. If both these convergence criteria are fulfilled, the solution is said to converge for that time increment, i.e. equilibrium has been obtained. ABAQUS then reads point *a* as if it is situated on the load distortion curve.

If one of the two given criteria for conversion is not fulfilled the iteration has not converged. The stiffness of the structure is then updated to $K_a$ which is valid for the point $u_a$. ABAQUS then performs a new iteration with the stiffness $K_a$ taken from the distortion $u_a$ in order to find a new balance of forces between the internal and the external forces (Figure 4.3). The stiffness together with the residual, $R_a$, determines whether a new distortion correction, $c_b$, shall be used which will take the system closer to equilibrium. If equilibrium is still not obtained another iteration will take place until the system converges.

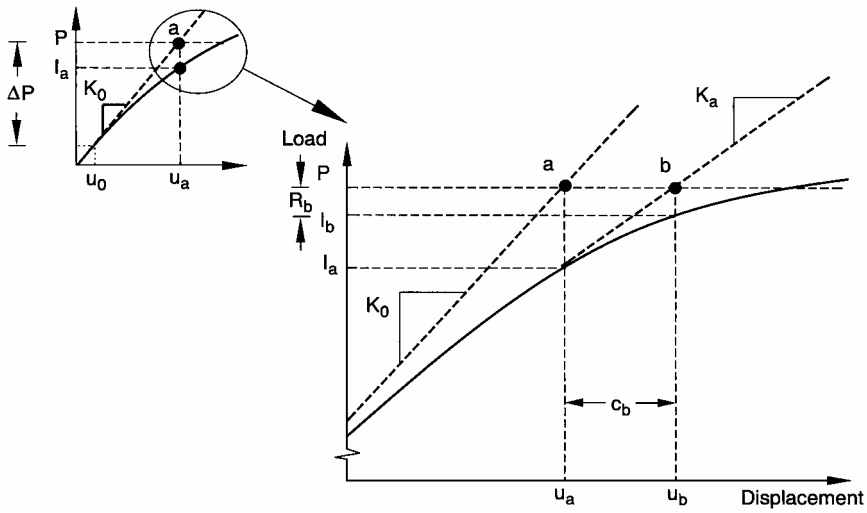


***Figure 4.3*** *Second iteration in a time increment (Hibbit et al, 1997).*

For each iteration in a non-linear analysis ABAQUS forms a stiffness matrix for the model and solves the system of equations. Each teration in a non-linear analysis therefore requires almost as large space in the computer and time for calculation as one complete linear analysis. This results in the fact that non-linear analysis requires much larger space than linear analysis.

## 4.3 Type of element

When modeling a problem in ABAQUS 5.7 a number of types of elements are available to build the model. Solids in one, two or three dimensions as well as specific structures in shape of shells etc can be modeled. Different elements are available for coupled problems as for example temperature and stress problems or effective stress and ground water flow problems. Figure 4.4 hows the most frequently used types of element for stress analysis. The important difference between the different families of elements is the geometry.

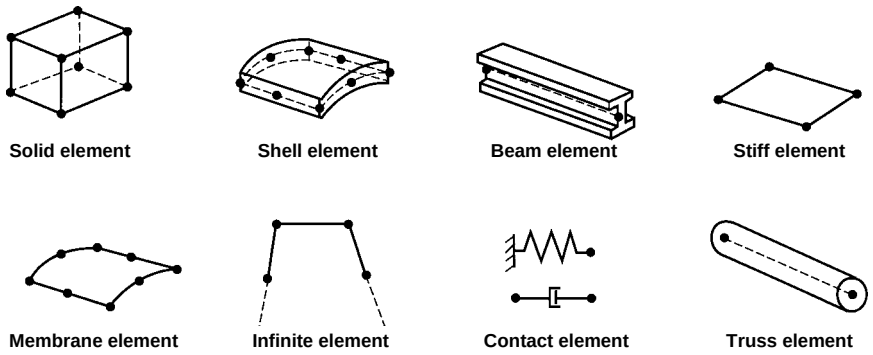


***Figure 4.4*** *Commonly used element types in ABAQUS (Hibbit et al, 1997).*

The degrees of freedom in a model are the basic variables, which are calculated during the analysis. During stress-strain analysis the deformations are the most important degrees of freedom and for shell and beam element the rotation for each node. For geotechnical analyses with elements, which can model pore pressure (so called two phase element) the pore pressure is an important degree of freedom for the nodes.

Deformation and other degrees of freedom are calculated for the nodes for one element. For the other points within the element the variables are integrated and interpolated from the values in the nodes. For a more detailed description of integration and formulation the reader is referred to ABAQUS/Standard User's manual (Hibbit et al, 1997).

When constructing the element mesh for a problem it is important to make a finer mesh within the most interesting part of the model and a coarser mesh in other areas. It is also of utmost importance to strive to keep the number of elements down when considering the time for calculation and the requested capacity of the computer.

For the analyses of the canister the solid elements were used for modeling the canister. The bentonite was also modeled with solid elements, which in this case could handle pore pressure (two-phase element). The friction between the canister and the bentonite and between the copper and iron part of the canister was modeled by contact elements (so-called interface element). Different properties for the different elements will be treated in the following sections.

### 4.3.1 Solid elements

For complicated geometry it is customary to use solid elements. They can be used for linear analyses as well as for complex non-linear analyses including contact element, plastic flow and large deformations. The solid element is a very useful type of element when analysing stress, heat flow, acoustic effects, coupled temperature stress and coupled pore water pressure and stress and piezo electric problem as well as coupled temperature electric problems. Figure 4.5 shows examples of a few different solid elements.

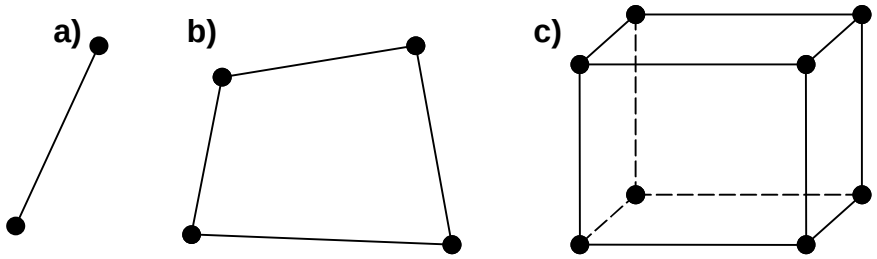


***Figure 4.5*** *Solid element in a) one dimension, b) two dimensions, c) three dimensions.*

The modeling with the help of solid elements usually means large amounts of calculations as all degrees of freedom are used. The accuracy of the calculations can to a great extent be directed by the user through choosing nodes and points of integration for the element.

### 4.3.2 Contact elements

The contact elements are used in order to model the contact between two different surfaces. There are different types of contact analyses. For stress strain analyses the interest is focused on what happens at the contact point between two surfaces. Between two surfaces in contact friction forces of varying size will develop. The friction depends on the friction coefficient ($\mu$), which can be modeled by means of contact elements. For certain cases the friction coefficient is so small that it can be neglected in the calculations, i.e. the surfaces are considered to be slick, and the friction coefficient is assumed to be zero. Full continuity between two surfaces corresponds to a friction coefficient equal to one. Contact elements are also used in order to stop two surfaces from penetrating into each other. There are several types of contact elements, which model the above conditions. The contact elements have no volume.

We have used two different types of contact elements. One to model surface based contact and the other to model the contact between elements. When modeling surface based contacts the phenomenon *contact pair* is used. In this case two surfaces are defined, which are required to be in contact. Contact model by contact elements often makes use of interface element or gap contact element (Figure 4.6). A detailed description of these can be found in ABAQUS/Standard User's manual (Hibbit et al, 1997).

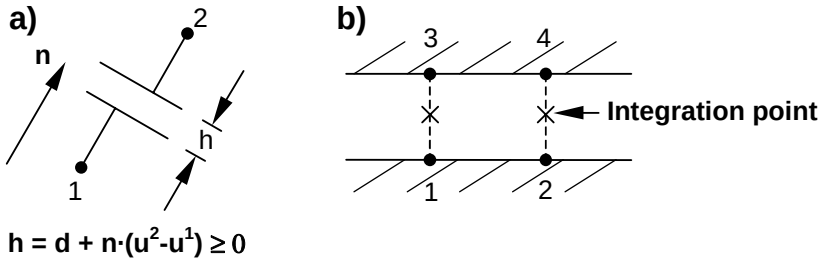


***Figure 4.6*** *Two types of contact elements: a) GAP-element, b) Interface element.*

## 4.4 Constitutive models

In ABAQUS/Standard 5.7 a number of constitutive models are given, from a simple linear elastic to non-linear elasto plastic models. Among these there are several models which are specifically suited for soil materials and are based on different yield criteria. These models are Drucker-Prager, Mohr-Coulomb and Cam-Clay/Critical state. For a detailed description of these and necessary material parameters the reader is referred to ABAQUS/Standard 5.7 User's manual I (Hibbit et al, 1997). For each model a certain alternative for material behaviour are available e.g. "hardening", "cap" etc. There is also a possibility of defining new material models to describe a certain material's behaviour with a better congruence than the predefined models.

# 5 Verification of analyses made with ABAQUS

## 5.1 General

Before modeling the full nuclear waste canister benchmark analysis were made in order to check the constitutive models for the material and the behaviour of the model in ABAQUS. By successively checking local models a good insight was obtained in how to model problems with ABAQUS. Local problems were analysed with another computer program and checked with theoretical hand calculations in order to verify the behaviour of the ABAQUS-model. The analyses were compared with calculations from PLAXIS and SIGMA/W, which are computer programs specially designed for geotechnical problems.

## 5.2 Check for material behaviour and computer code

### 5.2.1 Deformation during triaxial testing

When investigating deformation properties for a soil material with the Cam-Clay model a consolidated, undrained triaxial test was modeled. An initial stress state was applied and then the vertical load was increased and deformation and pore pressure buildup was observed. The model was built as a simple model with one single 8-node axialsymmetric element with four integration points. An initial cell pressure of 100 kPa was applied on the element and the initial pore pressure was set to zero. Thereafter the vertical load was increased by 50 kPa.

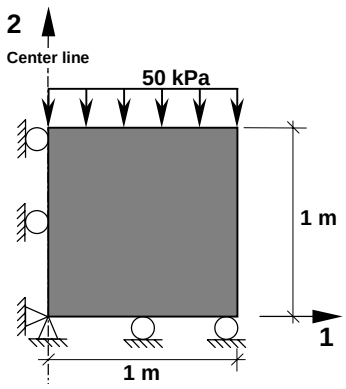


***Figure 5.1*** *Axisymmetric triaxial test.*

The soil properties used in the Cam-Clay model are given in the table below (Table 5.1).

***Table 5.1*** *Material properties for triaxial testing.*

| | |
|---|---|
| **Elastic parameters** | |
| Logarithmic bulk modulus, $\kappa$ | 0.026 |
| Poisson's ratio, $v$ | 0.3 |
| **Plastic parameters** | |
| Logarithmic hardening modulus | 0.174 |
| Critical state number (circular yield surface), $M$ | 1.0 |
| Initial preconsolidation parameter, $a_0$ | 58.3 kN/m$^2$ |
| Initial void ratio, $e$ | 1.08 |

The effect of an external load is a deformation of the element and the buildup of the pore pressure.

Analysis of the problem by ABAQUS gave deformations and pore pressures according to the table below. In order to compare the computation the same analysis was made with PLAXIS. In Table 5.2 the results are compared from these two calculations.

***Table 5.2*** *Comparison between ABAQUS- och PLAXIS- calculations.*

| | $\varepsilon_{11}$ | $\varepsilon_{22}$ | **Pore pressure, $u_{till}$, (kPa)** |
|---|---|---|---|
| ABAQUS | 0.00328 | 0.00656 | 25.6 |
| PLAXIS | 0.00347 | 0.00703 | 29.5 |

The results from the calculations in ABAQUS and PLAXIS differ somewhat from each other. The reason for this is probably that the geometric model is far too simple, i.e. with only *one* element. When using a small number of calculation points (nodes and integration points) the accuracy in the calculations become somewhat less, due to that larger approximations between the points of calculations are necessary. The method for solving this is different for different FEM programs, which can be noted when large approximations are used in simple models. A finer mesh gave far better correspondence for the results of the calculations.

The element mesh was somewhat different for the two analyses. In PLAXIS primarily triangular elements are used. For this model two elements were needed with 15 nodes each in order to model the same model as ABAQUS 8-node element (Figure 5.2).

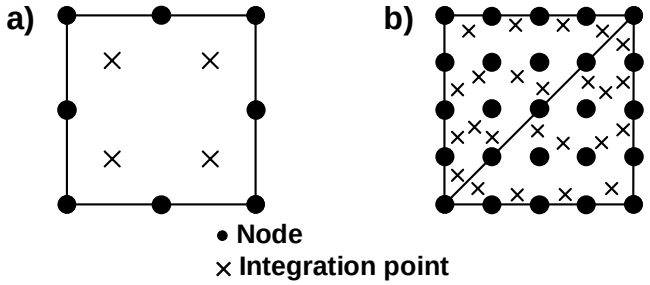


***Figure 5.2*** *Element: a) ABAQUS-analysis, b) PLAXIS-analysis.*

The results from the ABAQUS-analysis were compared with the PLAXIS-analysis for exactly the same strain. This was accomplished by prescribing a vertical distortion, $u_{2,}$ on top of the model instead of a distributed load. The applied deformation corresponded to the deformation obtained for the PLAXIS-calculation for the previous problem ($u_2$ = 0.00703 m). This gave a response that was *completely* in coordinance with the PLAXIS-analysis.

### 5.2.2 Triaxial test using Cam-Clay

It is interesting to investigate the case where a constitutive material model in ABAQUS is subjected to a load exceeding the failure load. In order to compare and evaluate the results from such analyses and state whether they are reliable or not and whether the models function as anticipated, a few other computer programs were used to do the analyses. The programs used were PLAXIS and SIGMA/W. Theoretical hand calculations were also made in order to evaluate the computer analyses.

The model in this case is very simple, i.e an 8-node axialsymmetric undrained element. Geometry and boundary conditions are given in the figure below (Figure 5.3) and is very similar to what was used in the previous analyses. The diameter of the sample however is only half of the case treated before.

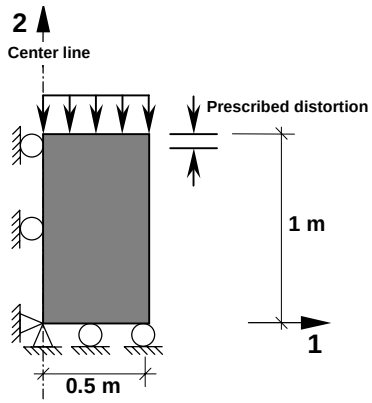


***Figure 5.3*** *Axisymmetric triaxial test for verification of failure mode – Cam-Clay.*

The geostatic state of initial stresses of 100 kPa was applied on the model at the same time as the initial pore pressure was set to zero. Thereafter a load was applied on top of the sample, large enough to bring the sample to failure. The interesting point in this analysis is to investigate how the stress state will be at failure. The properties of the material model are given in the table below.

***Table 5.3*** *Material parameters for the triaxial test.*

| | |
|---|---|
| **Elastic parameters** | |
| Logarithmic bulk modulus, | 0.05 |
| Poisson's ratio, *v*: | 0.3 |
| | |
| **Plastic parameters** | |
| Logarithmic strain hardening | 0.3 |
| Critical state number, *M*: | 1.0 |
| a) Preconsolidation ratio, | 1.25 |
| $\Rightarrow$ Preconsolidation | 62.5 kPa |
| b) Preconsolidatin ratio, | 5 |
| $\Rightarrow$ Preconsolidation parameter, $a_0$ | 250 kPa |
| Initial void ratio, *e*: | 3 |

Two different analyses were made with two different values on the overconsolidation ratio (OCR), 1.25 and 5.0 respectively. The preconsolidation ratio was defined according to the following equation.

$$OCR = \frac{\sigma_c}{\sigma_0} \qquad (5\text{-}1)$$

This implies an OCR value of 1.25 and initial stress of 100 kPa corresponding to a preconsolidation stress of 125 kPa.

In case when the preconsolidating stress was 125 kPa and the vertical load successively was increased the stress situation in the model was on "the wet-side" of the Critical state line. The stress path for the different FEM-analyses during loading is given in diagram 5.4 and can be compared.

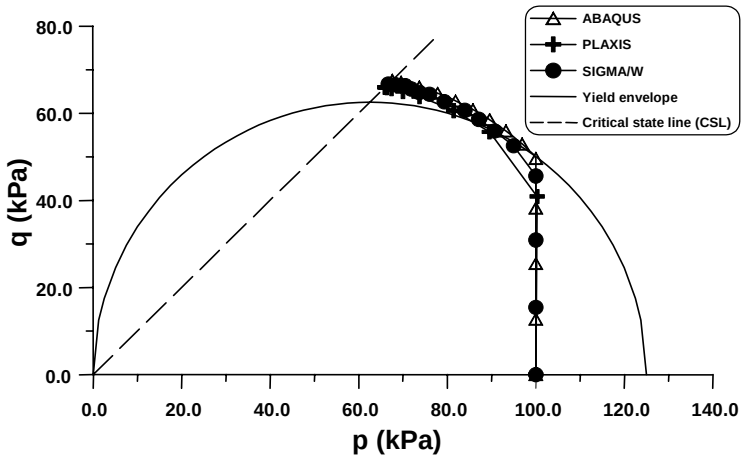


***Figure 5.4*** *Comparison between the stress path to failure for undrained triaxial test on "the wet-side" of the Critical state line for different computer programs.*

During the analysis of the overconsolidation ratio of five (*OCR* = 5), i.e. the preconsolidation stress was equal to 500 kPa for the initial stress of 100 kPa, a few complications occurred in ABAQUS. The stress path was terminated when the deviator stress reached its top value without failure having occurred, i.e. reached the *Critical state line*. Instead of applying a uniformed stress in order to bring the material to failure a large vertical deformation was applied on the model. The effect of this however resulted in a stress path beyond failure and the results corresponded well with the other programs.

The stress paths up to failure for the different computer analyses are given and can be compared in the diagram below (Figure 5.5). The stress path in this case is situated on the "dry-side" of the Critical state line.

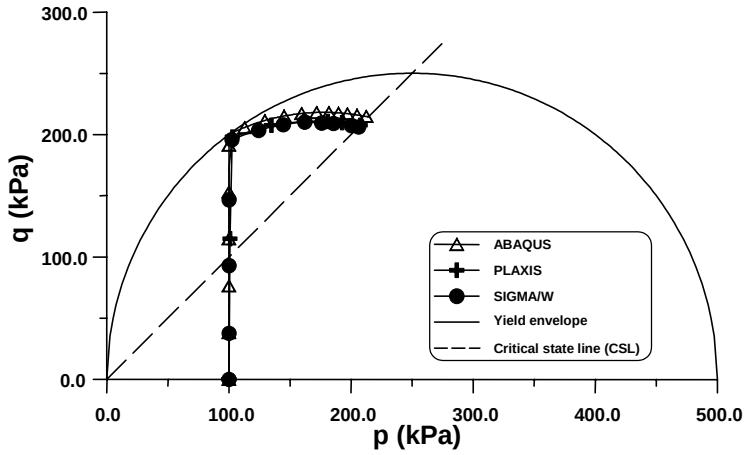


***Figure 5.5*** *Comparison between the stress path to failure for undrained triaxial test on the "dry-side" of the Critical state for different computer programs.*

The summary of the stresses at failure for the material, with the two cases with the different computer analyses, is given in the table below (Table 5.4).

***Table 5.4*** *Comparison between failure stresses for the undrained triaxial case with ABAQUS, SIGMA/W and PLAXIS.*

| | **Theoretical (kPa)** | **ABAQUS** | **SIGMA/W** | **PLAXIS** |
|---|---|---|---|---|
| Wet (Fig. 5.4) | 65.9 | 67.6 | 66.7 | 66.0 |
| Dry (Fig. 5.5) | 209.1 | 214.3 | 206.1 | 207.5 |

Table 5.4 shows a good correlation between the analyses from the three computer programs, where the deviation is at the most 2-4 %.

### 5.2.3 Check of a number of ABAQUS statements

In order to create models that coincide well with a real problem it is important to master the different parts of the finite element program which can be used. Several, fairly simple analyses were therefore performed in order to investigate how geometry, friction, geostatic initial stress (initial stress in the material which do not result in any strains), drainage, pore pressure etc were modeled in ABAQUS. When these problems were investigated and code was found to function well they were linked together to a more complex problem in order to finally model the canister being used for repository.

It is our opinion that the ABAQUS-calculations function well and that the material properties used were well modeled in the ABAQUS-program.

# 6 The Finite Element Model

## 6.1 General

In order to be able to perform analyses of the effect of stresses and deformations caused by external factors on the canister a somewhat simplified computer model of the canister and its surrounding had to be created. The purpose with the model is to simplify the real problem to a model with corresponding behaviour where stresses, deformations etc can be simulated and analysed. When constructing such a model of a finite element model it is important to have, in depth, knowledge about geometry and the material parameters that govern the behaviour of the model.

## 6.2 Geometry

The geometry of the canisters according to the KBS-3 concept has been copied from drawings and information obtained from SKB.

The inner part of the canister consists of a cast iron insert, which constitutes the canister's mechanical protection around the nuclear elements. The geometry for the cast iron insert is given in Figure 6.1. A 50 mm thick copper shell surrounds the iron insert.

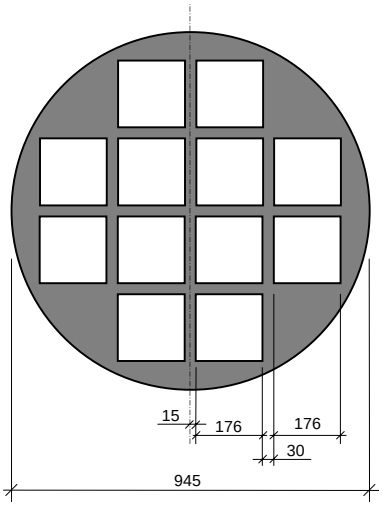


***Figure 6.1*** *Geometry for the cast iron insert.*

The canister has a diameter of 1045 mm and a total length of 4830 mm. The hole, which is drilled in the bedrock for deposition of the canister, will have a diameter of 1.5 m and a depth of 7.5 m. The following figure shows the position of the canister in the deposition hole when it is surrounded by bentonite.

Other designs for the canister have been discussed (Werme, 1998). These designs are named BWR and PWR. The latter only marginally deviates in the geometry from the design given in Figure 6.1. and has a bending stiffness of about 12 % larger. Thus the results from calculations for the geometry in the BWR canister would result in slightly lower strains and thus also slightly lower stresses. The PWR canister has a bending

stiffness of about 17 % higher than the BWR canister and will thus develop even smaller strains.

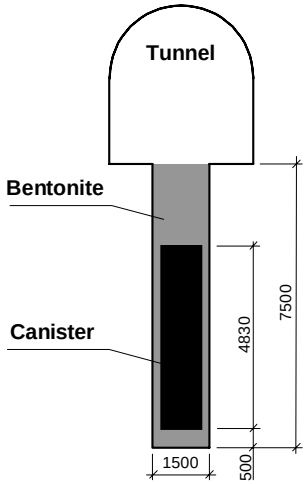


***Figure 6.2*** *Dimensions for the canister and the deposition hole.*

When making a finite element method model of the canister and the bentonite the symmetry in geometry is used and a plane of symmetry is placed through the central axis of the canister. It is therefore only necessary to model one half of the canister and the deposition hole. The canister will then obtain the shape of a half circle.

The cast iron insert of the canister has a complicated geometry, which results in a complicated FEM-modeling. In order to simplify the modeling, the cast iron insert, initially was replaced by an equivalent iron insert having the shape of a cylinder with the same moment of inertia as the true iron insert. This means that the insert gives the same response during bending as the true canister. The thickness of the equivalent iron insert was determined to be 98 mm. If pure shear of the canister is studied a thickness of 128 mm of the equivalent iron insert is required in order to give the same shear resistance as for the true insert. When modeling the insert a thickness of 98 mm was chosen as the critical case as was found from calculations of inertia. The model was analysed as being extended half a meter above the canister. The effect of modeling the full deposition hole gives according to preliminary analyses only marginal effects on the stresses in the canister.

## 6.3 Elements and element mesh

When modeling a canister and the surrounding bentonite, three-dimensional solid elements were used. In ABAQUS a number of different types of solid elements are available which are specially suited for different types of analyses. For the canister a stress-strain element was chosen and for the bentonite which is modeled as a two phase material, i.e. it consists of solid particles and pore water, a pore pressure element which can simulate the effect of pore pressure and stresses in the element was chosen.

The solid element chosen has 20 nodes with three degrees of freedom, i.e. deformation in x-, y- and z-direction can occur. In order to minimize the computation time the numbers of integration points[1] were reduced, i.e. the number of points in the element for which stresses are integrated and interpolated. Sensitivity analyses show that this will give sufficient accuracy in the results. The element name for the two different solid elements used are C3D20R and C3D20RP respectively, where R defines reduced number of integration points and P defines pore pressure element. The geometry of the nodes for the 20-node solid element is given in Figure 6.3.

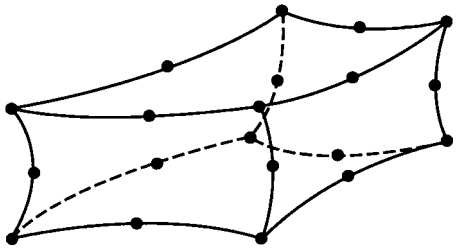

***Figure 6.3*** *Three-dimensional 20-node solid element with reduced number of integration points (Hibbit et al, 1997).*

The contact between the bentonite and the canister and copper and iron were modeled with 16-node interface element, so called INTER8. The configurations of these are given in Figure 6.4. The reason for choosing the interface element instead of for example GAP-element or contacts is that the interface element can model contact between pore pressure element and stress-/strain elements.

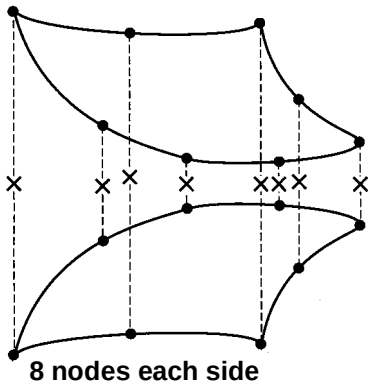


***Figure 6.4*** *16-node interface element (Hibbit et al, 1997).*

The size of the elements in the model varies a lot depending on the position of the elements in the model. Relatively small elements are located close to the shear plane or at contact regions between two different materials. The reason for this is that these areas are especially interesting parts of the models where stresses and strains vary locally and can become large. In order to avoid numerical problems for the model it is favourable with smaller elements, which means fewer approximations in the calculations in these areas. When constructing the element mesh it is also important that the width-length

[1] The number of integration points in the element was reduced from 54 to 24.

ratio for the element is not too large. If the ratio of length to width is too large very slim elements are obtained with possibilites of numerical problems as a result. The ideal element form for a solid element is cubic. The element mesh for the canister and the surrounding bentonite is given for the equivalent model in Figure 6.5.

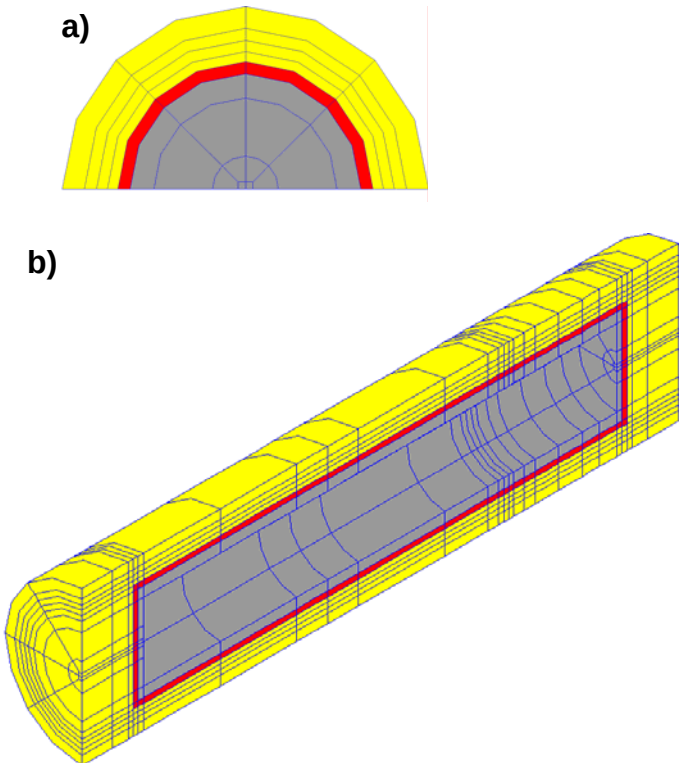


***Figure 6.5*** *Element mesh for the model: a) section, b) three-dimensional.*

The element mesh in the ABAQUS model was chosen according to Figure 6.5. When constructing the element mesh the nodes which constitutes the element are defined. When generating the element you start with a defined element, a so-called *master element* and give the node number increase for the corresponding nodes on the "new" element. It is therefore important that before building the model a logical and simple node numbering is chosen so that the corresponding nodes in different elements have the same internal node number increase.

## 6.4 Material parameters

The material properties for the materials in the FEM-model are defined through laboratory tests and earlier investigations and calculations of the canister which were performed by Clay Technology AB (Börgesson, 1992). After elaborate testing, the parameters describing the material properties were determined by Clay Technology. This is a very important part of the analysis as these parameters will be the base for the calculations and the results.

### 6.4.1 Bentonite

In the earlier calculations made by SKB on the canisters, bentonite was modeled with an extended Drucker-Prager model, which like Mohr-Coulomb's model can model different compression and tension stresses simultaneously. The elastic part of the material model was modeled as porous elastic. This means that the relation between the void ratio and the logarithm of the mean effective stress is a straight line and defined according to equation (6-1), see the Cam-Clay chapter.

$$\kappa = \frac{\Delta e}{\Delta \ln p} \qquad (6\text{-}1)$$

The elastic parameters for the material are thus $\kappa$ och Poissons's ratio $\nu$.

| | |
|---|---|
| Elastic material parameter, $\kappa$ | 0.21 |
| Poisson's ratio, $\nu$ | 0.4 |

The plastic behaviour of the bentonite accounts for, according to Drucker-Prager model, the internal friction, ($\beta$) and cohesion ($d$). The plastic behaviour is confined to the area between the yield surface and the failure surface, Figure 6.6. The increase in volume of the material during deformation, dilatation, is modeled by the angle of dilation ($\psi$) and the ratio between triaxial compression stress and tension stress as described in the extended Drucker-Prager model by the factor $K$. For the classical Drucker-Prager model $K$=1, i.e. the effect of simultaneous compression and extension in the model is equally large. The flow function for the bentonite, i.e. the plastic strain ($\varepsilon_{pl}$) as a function of the deviator stress ($q$), is described by a non-linear function according to Figure 6.6.

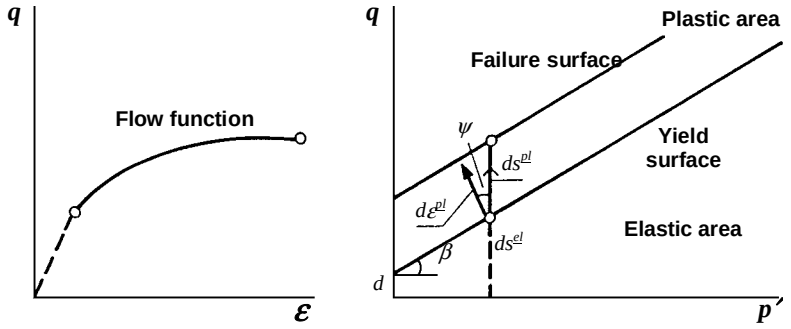


***Figure 6.6*** *Drucker-Pragers model for plasticity and non-linear yield function (Börgesson, 1992).*

The material properties describing the plastic properties of the material according to Drucker-Prager's extended model were determined through triaxial test on Na-bentonite MX-80 and are given below (Börgesson, 1992).

| | |
|---|---|
| Angle of internal friction, $\beta$ | 20° |
| Cohesion, $d$ | 100 kPa |
| Angle of dilation, $\psi$ | 2° |
| Ratio compression-tension, $K$ | 0.9 |

The flow function for the bentonite is given in the table below

| $\sigma_y$ (kPa) | $\varepsilon_{pl}$ |
|---|---|
| 113 | 0.0 |
| 138 | 0.005 |
| 163 | 0.02 |
| 188 | 0.04 |
| 213 | 0.1 |

where $\sigma_y$ is the failure deviator stress for Drucker-Prager model according to ABAQUS. The relation between $\sigma_y$ and the cohesion $d$ is described according to the equation below

$$\sigma_y = \frac{d}{1 - \frac{1}{3} \cdot \tan\beta} \qquad (6\text{-}2)$$

Hydraulic conductivity ($k$) in the bentonite varies with the void ratio ($e$) according to the following table.

| $e$ | $k$ (m/s) |
|---|---|
| 0.45 | $1.0 \cdot 10^{-14}$ |
| 0.70 | $6.0 \cdot 10^{-14}$ |
| 1.00 | $3.0 \cdot 10^{-13}$ |

### 6.4.2 Copper

The copper shell in the canister has been modeled with a three-dimensional linear elastic model described by the modulus of elasticity ($E$) and Poisson's ratio ($\nu$).

| | |
|---|---|
| Modulus of elasticity, $E$ | $114 \cdot 10^6$ kPa |
| Poisson's ratio, $\nu$ | 0.35 |

The plastic strain ($\varepsilon_{pl}$) is described by the flow function below in the same way as for the Drucker-Prager model.

| $\sigma_y$ (kPa) | $\varepsilon_{pl}$ |
|---|---|
| $50 \cdot 10^3$ | 0.0 |
| $80 \cdot 10^3$ | 0.015 |
| $130 \cdot 10^3$ | 0.065 |
| $180 \cdot 10^3$ | 0.154 |
| $210 \cdot 10^3$ | 0.288 |

### 6.4.3 Iron

The mechanical behaviour of the iron part of the canister is modeled with a traditional linear elastic model.

| | |
|---|---|
| Modulus od elasticity, $E$ | $200 \cdot 10^6$ kPa |
| Poisson's ratio, $\nu$ | 0.30 |

The flow function defining the plastic strain ($\varepsilon_{pl}$) is given in the following table.

| $\sigma_y$ (kPa) | $\varepsilon_{pl}$ |
|---|---|
| $300 \cdot 10^3$ | 0.0 |
| $412 \cdot 10^3$ | 0.023 |
| $542 \cdot 10^3$ | 0.078 |
| $697 \cdot 10^3$ | 0.147 |

### 6.4.4 Properties at the interface

Laboratory testing (Börgesson, 1990) has revealed the properties of the contact between the canister and the surrounding bentonite material. The testing has shown that no sliding occurs until a critical value of shear stress is reached. Thereafter the shear resistance is practically constant as long as the normal stress remains unchanged. This behaviour can be described with the Mohr-Coulomb parameters cohesion ($c'_c$) and friction ($\phi'_c$). The ratio between the angle of internal friciton and cohesion in the areas of contact compared to the bentonite are given below.

| | |
|---|---|
| Cohesion in the area of contact, $c'_c$ | $0.6c'_b$ |
| Angle of internal friction at the area of contact, $\phi'_c$ | $0.6\phi'_b$ |

Where $c'_b$ denodes cohesion and $\phi'_b$ is the angle of internal friction in the bentonite with Mohr-Coulomb parameters.

## 6.5 Loads

The loads during the finite element analysis are modeled according to possible external factors that can affect the canister and its integrity. The following cases have been studied

- tectonical movements in the bedrock which through cracks/fractures can expose the canisters to unwanted changes in stress
- the effect of possible irregular local swelling of the bentonite.

The modeling of tectonical movement in the bedrock was performed by assigning nodes describing the bedrock a disposition above a certain plane (Figure 6.7) constituing a shear plane. The position of the shear plane was varied to different levels of the canister. From earlier analyses of the canister it was known that the shear plane situated in the vicinity of one forth from the bottom results in the most dangerous loading case. The size of possible movements in the bedrock is impossible to estimate but during the analyses the effects of a movement of the bedrock of 10 cm during a time period of 30 days were modeled. During the consolidation calculation it is important that the steps in the analysis fulfil the following requirements, according to Vermeer and Verrulit (1981):

$$\Delta t \geq \frac{\gamma_w}{6Ek}(\Delta h)^2 \qquad (6\text{-}3)$$

as you otherwise may run into numerical problems with undulating results which do not reach a stable solution.

The movement of the bedrock in the shear plane results in a load that exposes the canister to bending. That is why the bending stiffness of the canister is critical for its strength.

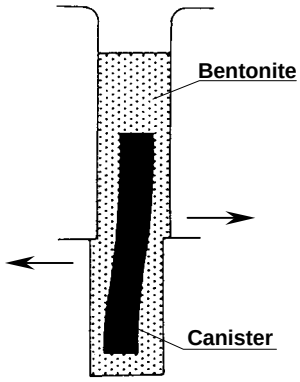


***Figure 6.7*** *Illustration of the tectonical movements in the bedrock and its impact on the canister (Börgesson, 1992).*

The effect of the gravitational forces on the canister and the bentonite was neglected as they can be regarded small compared to the stresses created by the swelling of the bentonite.

The result of the swelling of the bentonite was modeled as an inital condition according to chapter 6.6. The bentonite was in this case assumed to be fully saturated in the full model which gives a homogeneous swelling pressure on the canister. Due to shear zones in the bedrock water can be transmitted unevenly to the bentonite. This can in an early stage of the swelling result in the fact that the bentonite locally gets a large swelling. An unfavourable combination of local swelling of the bentonite around the canister could possibly give high stresses and deformations in the canister. Areas with local swelling can be compared with concentrated loads on the canister.

The modeling of local swelling of the bentonite depending on its swelling properties is possible to model in ABAQUS. It is however a relatively complicated problem. This is the reason to simplify the problem by describing a local impression on the model. An area of 30×30 cm was given a distortion inwards towards the canister (Figure 6.8). This

simplification and the effect of it gives a corresponding picture of what the critical stresses in the canister can be and thus a base for deciding whether it can threathen the integrity of the canister. The size of the impression has been chosen with respect to the stresses that the impression generates and the stresses shall be of the same order of magnitude as the swelling pressure that can be generated for the densities and water ratios considered.

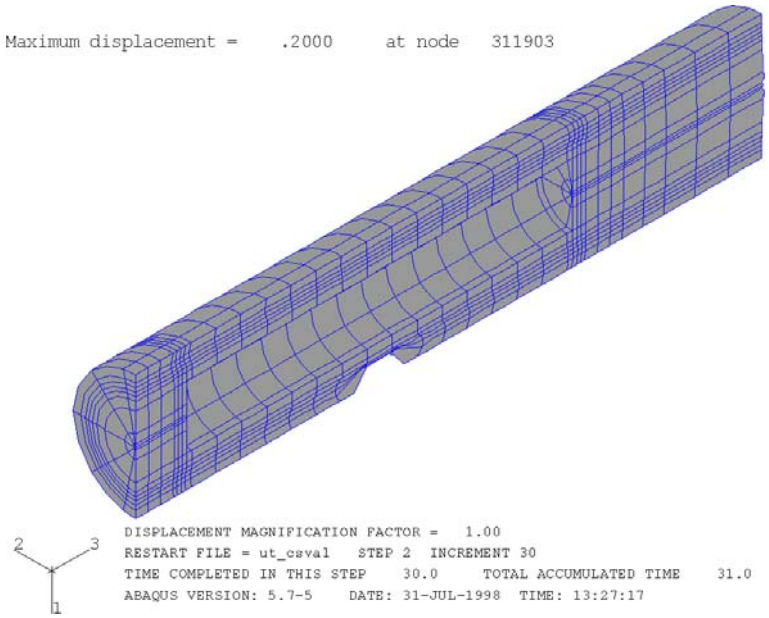


***Figure 6.8*** *Modeling of local swelling of the bentonite by impression of an area of 30×30 cm$^2$.*

# 6.6 Initial conditions

During the finite element analysis a number of initial conditions are defined which corresponds to the state of stress at hand in the model at start.

During the analysis the bentonite is assumed to be saturated which has resulted in severe swelling. Due to this swelling large swelling pressures develop in the bentonite. These stresses are substantially larger than those generated by the gravity forces and this is the reason why the gravity forces can be neglected in the calculations. From laboratory tests performed, by Börgesson et al (1995), the initial mean effective stress ($p'_0$) was determined for the model. The elastic behaviour of the bentonite and the permeability depends on the void ratio ($e$), which is the reason why also the initial void ratio ($e_0$) after swelling was determined through laboratory tests. When the canister is situated at a depth of 500 m below the ground surface the inital pore pressue in the bentonite was set to 5000 kPa, which corresponds to the hydrostatic effect of 500 m of water. The governing inital conditions used are given in the following table.

| | |
|---|---|
| Mean effective stress, $p'_0$ | 8000 kPa |
| Pore pressure, $u_0$ | 5000 kPa |
| Void ratio, $e_0$ | 0.65 |

## 6.7 Boundary conditions

Modeling of the canister and its surrounding has been limited to the bentonite and the canister. Where the FEM-model is terminated boundary conditions are introduced for the purpose of modeling the corresponding effect of the surrounding material. In this case it is the effect of the bedrock on the canister which is modeled through boundary conditions. The bedrock is assumed to be stiff, which in the model is modeled by the degrees of freedom for the outer nodes which describes the bedrock. These are locked against movement in x-, y- and z-directions. The contact between the bedrock and the bentonite is modeled as full interaction, i.e. full friction, which means that the locked nodes which constitute the bedrock also are part of the outer layer of the bentonite. At the top of the model the boundary conditions were given so that no vertical movements would occur into the above-situated tunnel. In the plane of symmetry for the canister the boundary conditions were that no deformation in y-direction occurs and thus can be described by a rolling boundary condition, see Figure 6.9.

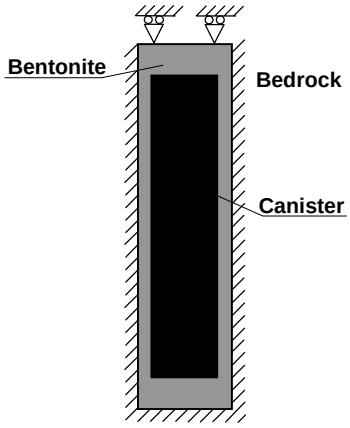


***Figure 6.9*** *Boundary conditions for the finite element model of the canister and the bentonite.*

During the analysis of the model undrained conditions have been assumed, which means that the boundaries were impermeable and did not allow for any out- or inflow of pore water in the model. A certain drainage would result in consolidation or swelling and result in a lowering of the stresses against the canister. Therefore the undrained case is considered as the most dangerous case.

## 6.8 Simplifications

In the finite element model analysed in ABAQUS certain simplification and approximation have been used in order to model the real problem in a reliable way. The purpose is that the model shall be simple and easy to use for computer analyses but at the same time model the real behaviour for stresses and strains. Simplifications, which are made in the computer model are described below.

- In order to minimize the calculations and time a plane of symmetry has been introduced in the model which means that only half of the canister is modeled in the FEM-analysis. The plane of symmetry corresponds in the model by that the deformation in y-direction is locked on the plane of symmetry.

- It is only the bedrock close to the bentonite which has been accounted for which means that the bedrock is assumed infinitely stiff. The elastic properties of the bedrock have therefore been neglected. The stiff bedrock was modeled by assigning no degrees of freedom for the nodes upon the boundary.
- The cast iron insert of the canister has been replaced by an equivalent cylindrically shaped iron insert with the same bending stiffness as the true insert. This means that the model becomes substantially easier to create and the size of the problem becomes smaller which results in shorter times for calculations.
- In the contact between the bentonite and the bedrock, friction has been assumed to be infinitely large which means that when the bentonite and the bedrock are in contact, they are fully connected and a possible failure will occur in the bentonite.
- The bentonite is assumed to be fully saturated which results in homogeneous swelling in the whole model.
- The different phases of swelling in the bentonite are not modeled. The resultning effect from swelling in terms of stresses, pore pressures and void ratios are given as initial conditions for the analysis. As the analyses have shown that no plastic deformations occur due to swelling this is considered a justified simplification giving the same effect on the canister.
- Gravitational forces on the canister and the bentonite are neglected in the analysis as they only constitute a neglectable part of the stresses in the model compared with the stresses generated by swelling.
- The model is assumed to be fully undrained which means that no pore water pressure can flow in or out over the boundaries. Analysis of a drained boundary at a constant pore pressure (5000 kPa) has shown that it results in a neglectable difference with the undrained case and is thus on the safe side.
- Comparison between this simplified model of the canister and a certain more rigorous modeling has been made seperately.

# 7 Analyses

## 7.1 General

The canister has been modeled in three different ways. In the first phase a shape was generated which is in accordance with an earlier geometry. The canister had in that case a diameter of 820 mm and a length of 4520 mm. The reason for creating this model was that detailed calculations for that model have been made by Börgesson (1992). The response by the model in the calculations can thereby be compared with earlier analyses in order to control or check that the model behaves correctly. After the results of these calculations had been checked the canister was modeled with the geometry that is used today. This model became rather large and resulted in times for calculation of approximately 48 hours due to the complex geometry of the cast iron insert. As a large number of analyses of the canister were planned calculation times of 48 hours were considered too long. Because of this a third equivalent model, with the same response as the true canister, where the iron insert was modeled as a cylinder was used. This model was used for the final analysis of the canister.

The most important results from the analyses are the following. The deviator stresses resulting in shear strains and thereby in possible plastic flow in the model.

## 7.2 Analyses and calculations

### 7.2.1 Old model

#### 7.2.1.1 Shearing in critical position

The first analysis peformed was shearing occuring one fourth from the bottom of the canister for a model where the original geometry for the canister was used. The canister was modeled as two cylinders with the same bending resistance as the true geometry and the true materials. Shearing of the canister was modeled by giving the nodes describing the bedrock above the shear plane a distortion according to Figure 7.1. The distortion assumed was given was 10 cm during a time period of one month, i.e. 30 days.

Stress and strains for the model due to the shearing of the bedrock coincides with the results from the analyses performed by Börgesson (1992). The used model is assumed to give a good picture of the canister. Pending deformation due to shear of the bedrock is given in Figure 7.2, where deformation has been enlarged ten times to better visualize what is happening. From the figure one can see large deformations occurring in the bentonite but the bending of the canister is moderate in the vicinity of the shear plane. The largest part of the bending occurs however in the centre of the canister where thus the largest stresses occur. Observe that the given deformations are enlarged and the true deformations are ten times smaller.

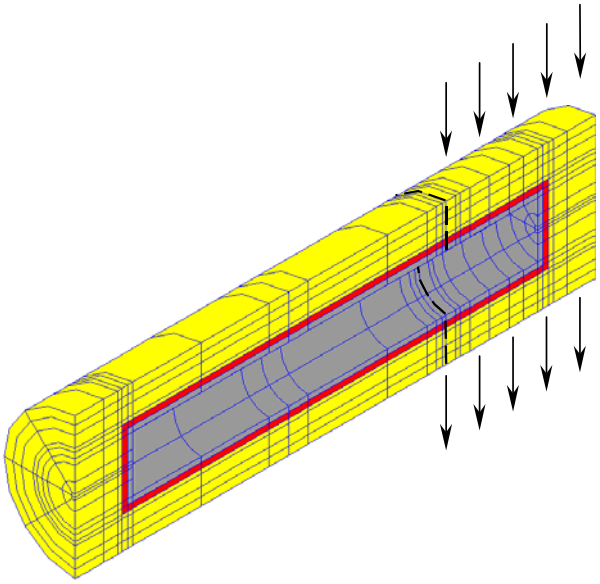

***Figure 7.1*** *Shear plane and movements of the bedrock in the critical position of the canister.*

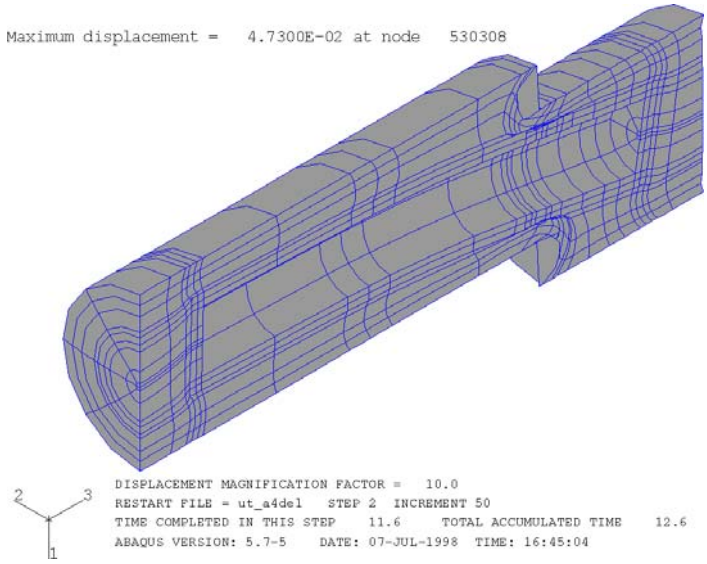


***Figure 7.2*** *Deformed model of 10 cm movement of the bedrock in a shear plane through the ciritical point. Deformation has been enlarged by a factor of 10.*

### 7.2.1.2 Shearing in the centre

In order to check that the position of the shearing plane is a critical loading case futher calculations were condected. These calculations gave lower deviator stresses in the canister (Figure 7.3), which means that the canister will be exposed to lower stresses compared to shearing in the critical section.

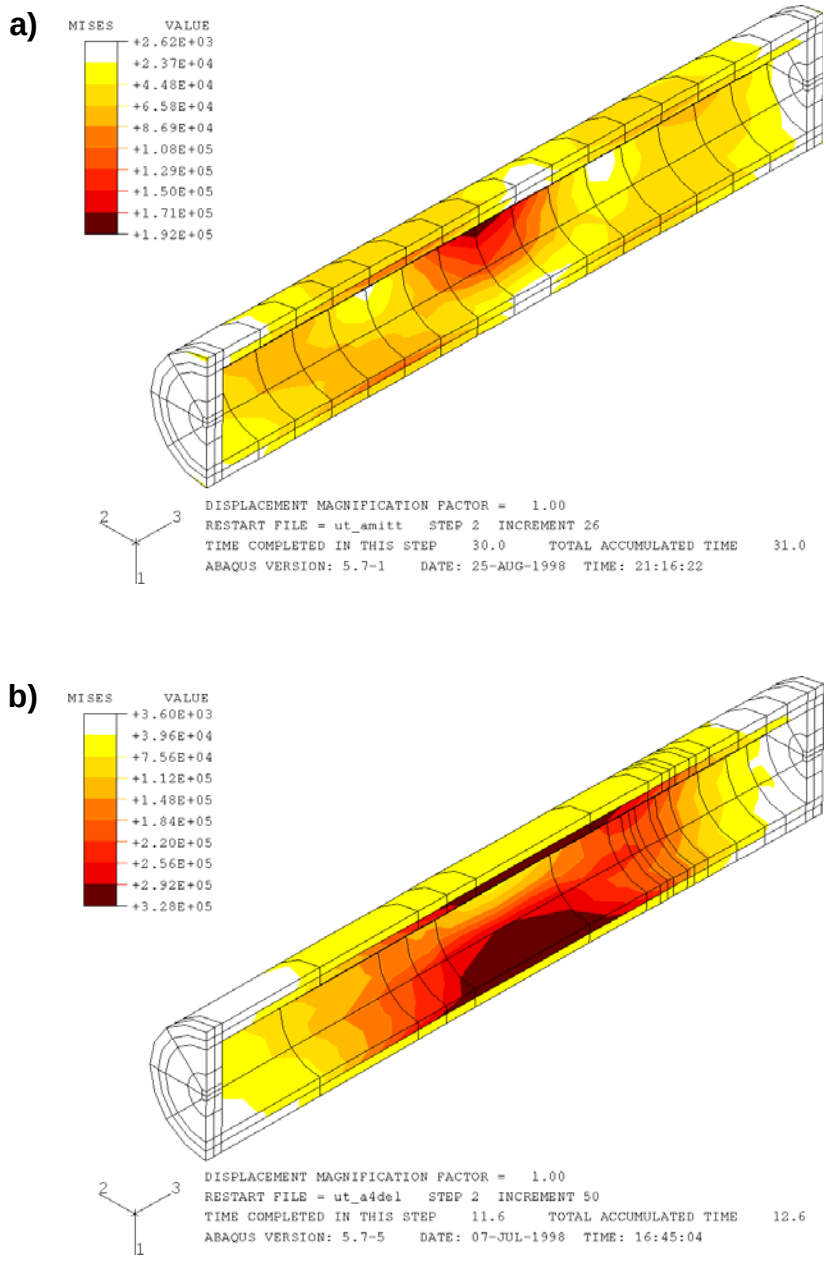


***Figure 7.3*** *Deviator stress (q) in the canister at shear in a) centre, b) one fourth from the bottom.*

### 7.2.1.3 Effect of shearing during incomplete swelling

In the previous described analyses the bentonite was assumed to be fully saturated with a homogeneous swelling in the whole model, as the shearing in the bedrock started to develop. The effect of swelling was modeled as an initial condition during the analysis of shear. If the tectonical movements in the bedrock are assumed to occur before the bentonite has been fully saturated and has undergone a complete swelling, this implies that the resulting stresses and pore pressures from the swelling phase will be smaller, which in turn means that the canister is not exposed to equally large initial stresses during the analysis.

Analysis of the effect of the initial stresses has been investigated for the canister. For example, initial stresses corresponding to one tenth of the original stresses gave a deviator stress according to Figure 7.4. This deviator stress can be compared with

deviator stresses from the original case according to Figure 7.3. The largest deviator stress is in the latter case, only 10 to 15 % of what was obtained with higher initial stresses, which shows that the higher the initial stresses are in the bentonite, the higher the stresses are in the canister.

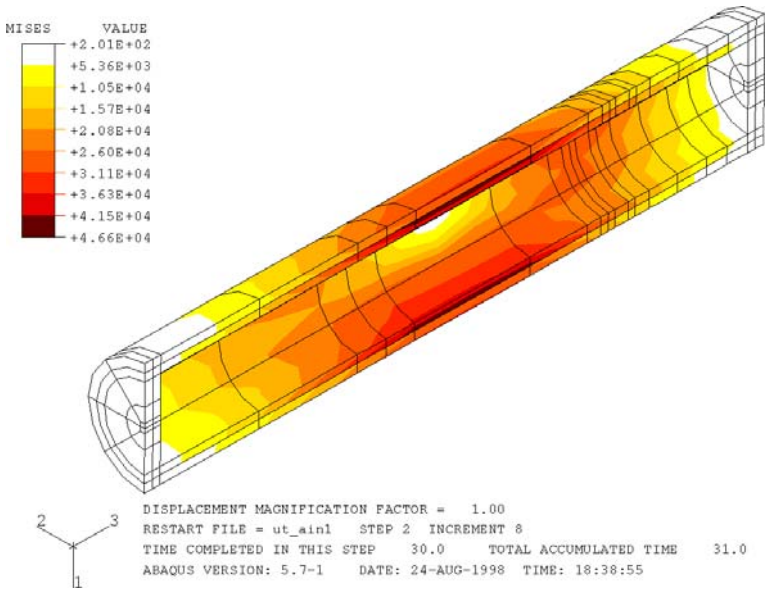


***Figure 7.4*** *Deviator stresses in the "old" model, with initial conditions corresponding to one tenth of the original, due to a shear of 4 cm of the bedrock in the critical section before swelling of the bentonite.*

## 7.2.2 Real model

### 7.2.2.1 Shear

The model of the canister with the real shape and the cast iron insert around the radioactive element includes a much larger number of elements and nodes than the equivalent model. A section of the model is given in Figure 7.5. This model resulted in extremely long calculation time and large the need of capacities during calculations. The contact between bentonite-copper and copper-iron was modeled as full correspondence effect, i.e. full friction.

During the analysis of the effects of a tectonical movement in the bedrock in the critical section this model is specially interesting to regarding stress concentration and yielding as result in the iron between the nuclear elements.

The deviator stresses which occur in the model due to a 5 cm movement of the bedrock is given in Figure 7.6.

A cross section of the model in the centre and in the critical section shows that there are no stress concentrations, resulting in severe plastic strain in the iron between the radioactive elements, according to Figure 7.8. However some plastic yield occur in the coppershell.

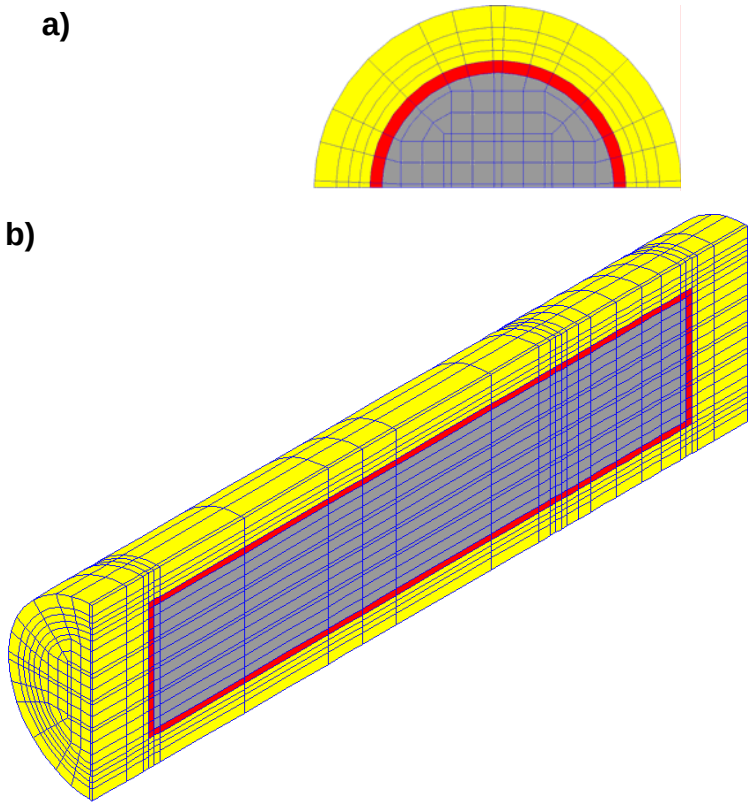


***Figure 7.5*** *Element mesh for a section of the canister with the correct modeling of the iron insert a) section, b) three-dimensional.*

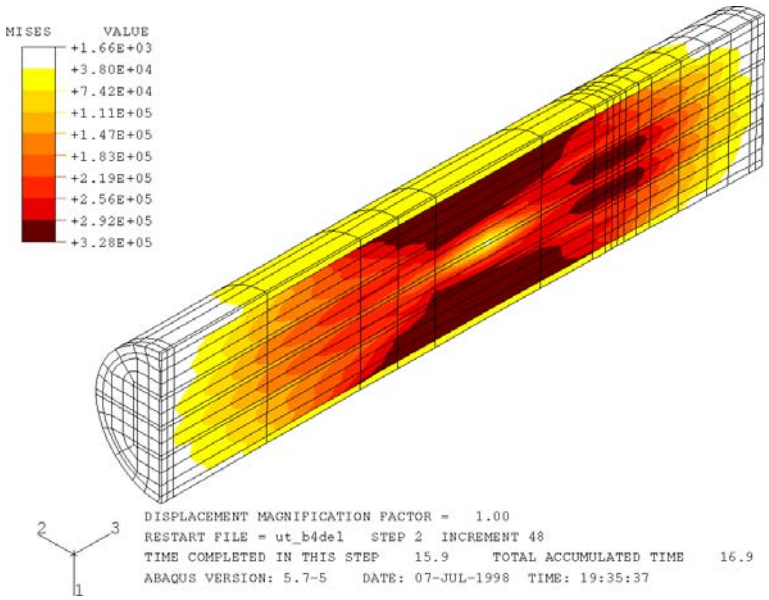


***Figure 7.6*** *Deviator stress in the canister in the true model after 5 cm shear of the bedrock in the critical section.*

a)

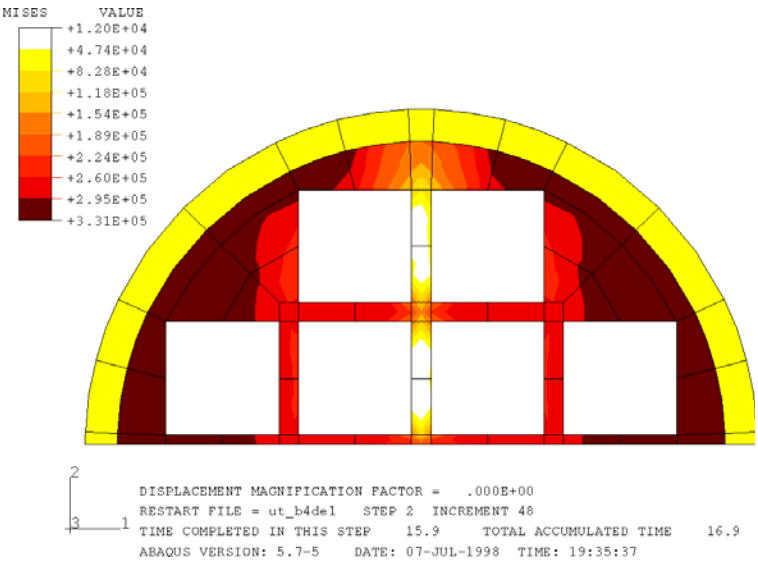


b)

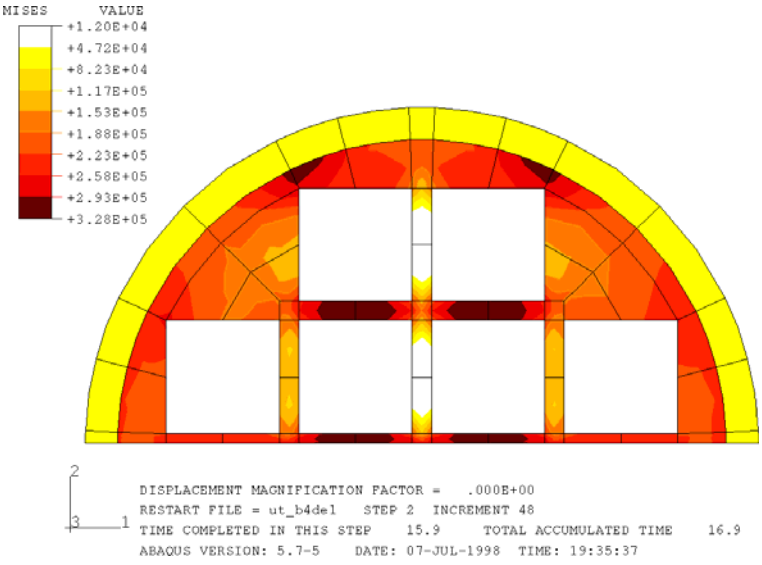


***Figure 7.7*** *Deviator stresses in the canister for the section in a) centre, b) critical section.*

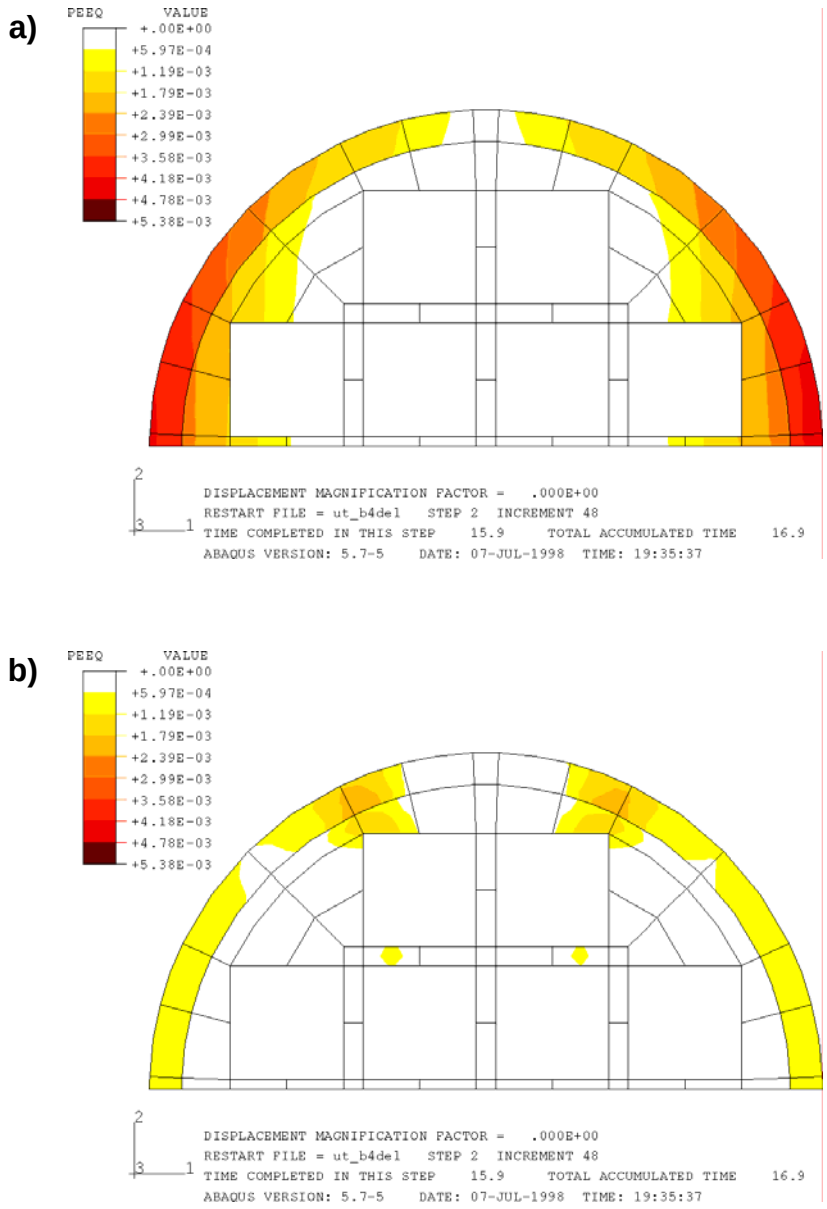


***Figure 7.8*** *Plastic deformation in the canister for section in a) centre, b) critical section.*

The analysis of the effect of movements of the bedrock results in large pore pressure changes in the bentonite as the analysis for the bentonite is performed as an undrained analysis. This very large pore pressure results in tremendous gradients, which in turn result in consolidation of the bentonite with accompanying strains. This in turn results in a relaxation of stresses and by this smaller stress in the canister. The undrained case is accordingly the most critical loading case and the corresponding stresses constitute an upper boundary. Pore pressure which exceed 13 MPa were generated on the compression side of the canister and negative pore pressures less than 19 MPa were developed on the corresponding side of the canister according to Figure 7.9.

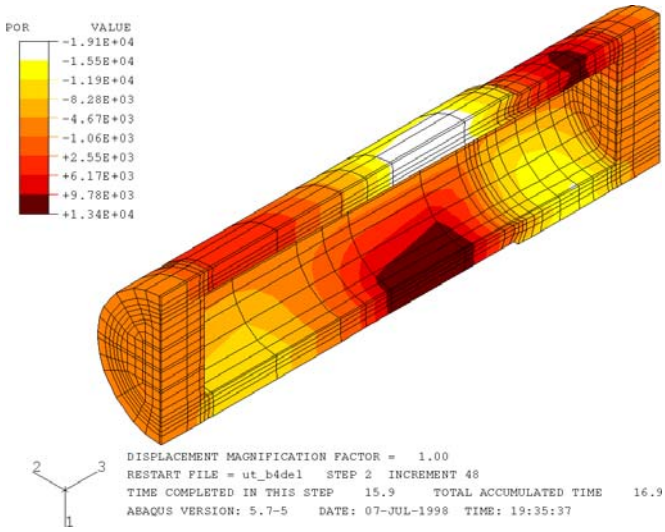


***Figure 7.9*** *Pore pressures (u) generated in the bentonite due to shear of the bedrock.*

## 7.2.3 Model for equivalent geometry

### 7.2.3.1 Shear

Shearing of the canister in the critical section for the model with an equivalent iron insert gives very good agreement with the model using the true iron insert. Stresses, deformations and pore pressures only marginally deviate from each other, which means that the equivalent iron insert is a worthy approximation of the true iron insert when it comes to stiffness, bending etc.

The effect of the assumed tectonical movements in the bedrock give only very small plastic strains in the canister (Figure 7.10). The canister will be exposed to its largest bending stresses approximately in the middle where thus the plastic strains first will occur.

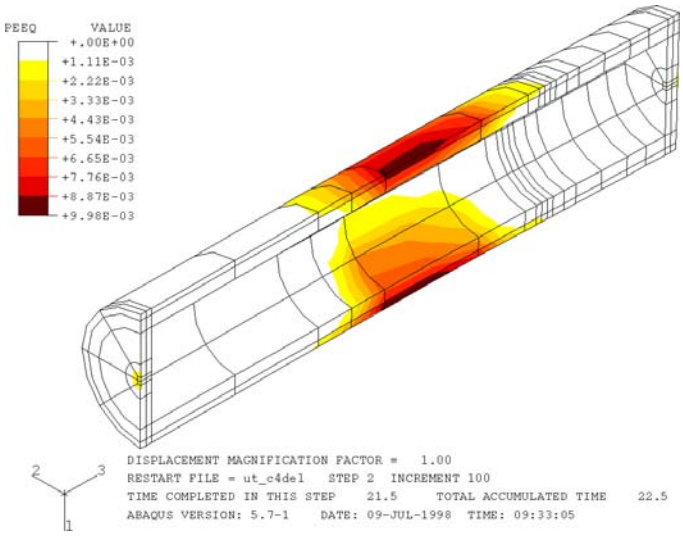


***Figure 7.10*** *Plastic straining of the canister due to 5 cm shear of the bedrock in the critical section for the equivalent canister.*

The magnitude of the plastic strains compared with the flow function and where on this flow function the strains are found is given in Figure 7.11. It can thus be seen how far away the material is from failure or how much of its shear strength remains as the material is deformation hardening.

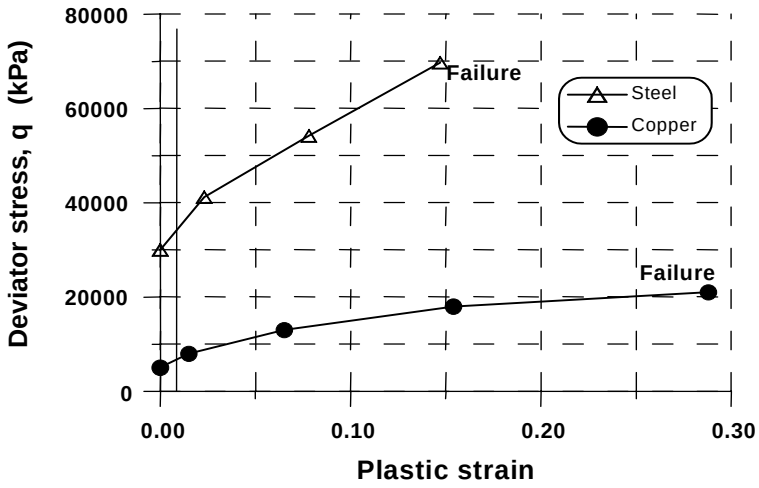


***Figure 7.11*** *Flow function for iron and copper with a full stress-strain curve for the plastically strained parts of the canister.*

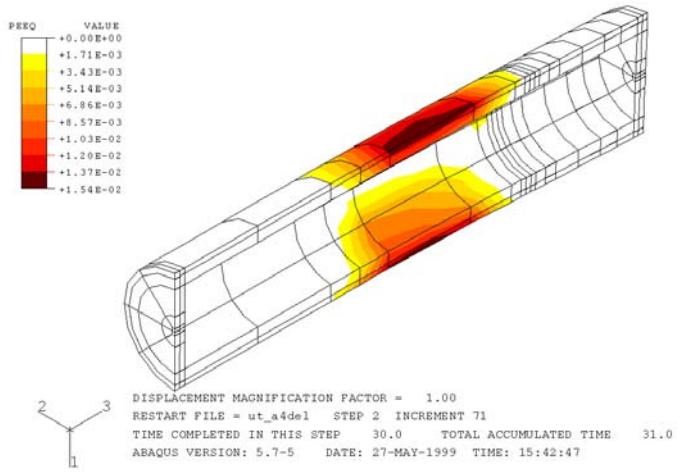


***Figure 7.12*** *Plastic straining of the canister due to 10 cm shear of the bedrock in the critical section for the equivalent canister*

Comparison with the flow function shows that the developed plastic strains are in the beginning of the flow functions. In order to bring the canister to failure substantially larger deviator stresses are necessary in the canister, which in turn requires much larger shearing deformation of the bedrock than 10 cm. See Figure 7.12.

### 7.2.3.2 Effect of finer element mesh and a movement of the boundary

The model of the canister and the bentonite consists of elements with varying sizes depending on which part of the model is regarded. The results from shearing in the critical section according to chapter 7.2.3.1 show that the canister will get the largest strains approximately in the centre where the plastic deformations also first occur. The element mesh in this part of the model is relatively coarse, which implies that the results of the calculations can be improved somewhat by changing the element mesh in this area. The result of expanding the model to include the full deposition hole above the canister, i.e. movement of the boundary to 2.5 m instead of 0.5 m above the canister, can also have certain effects on this state of stress as possible boundary condition otherwise can effect the canister. Modification of the element mesh and the boundary is given in Figure 7.13.

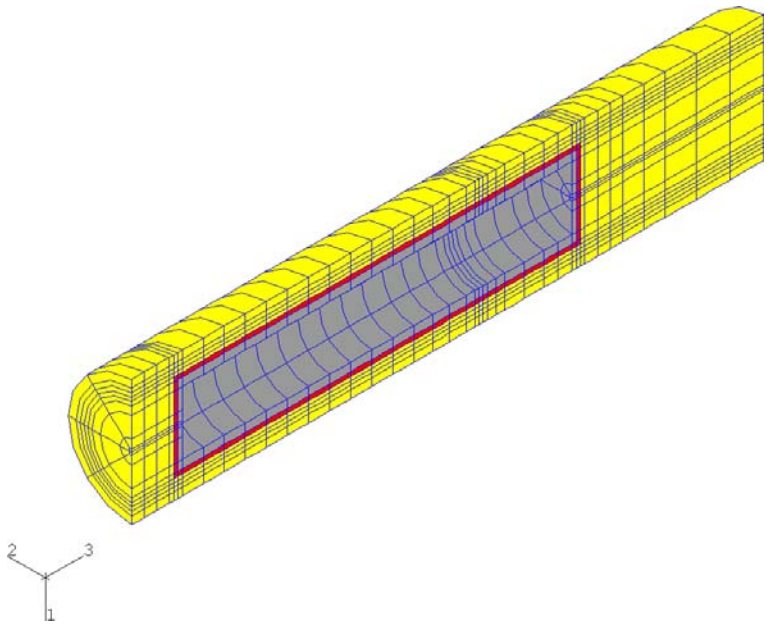


***Figure 7.13*** *Refined element mesh modeling for the canister and expansion of the boundary.*

A modification of the model according to Figure 7.13 results in only marginally larger stresses and plastic strains in the canister compared to shear in the critical section. This is shown in Figure 7.10 and Figure 7.14. The plastic strains that occur are still too small to create a threat to the integrity of the canister (Figure 7.11).

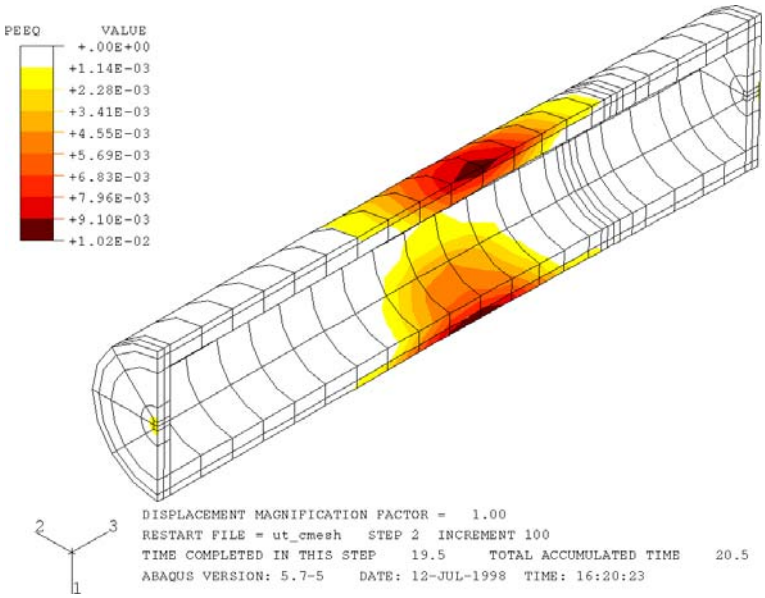


***Figure 7.14*** *Plastic deformation of the canister after refined element mesh and expansion of the boundary.*

### 7.2.3.3 Friction

The analyses above of the canister, assumes full interaction between the bentonite-copper and copper-iron elements. The properties of the contacts determined from laboratory tests have not been used and instead full interaction has been assumed. When modeling the contact properties with interface elements it was discovered that ABAQUS has limitations and only can define friction through a friction coefficient ($\mu$). The properties determined in the Mohr-Coulomb parameters could therefore not be modeled. When analysing the effect of the friction in the contact areas the two extremes were modeled, i.e. $\mu = 1$ (full interaction) and $\mu = 0$ (slick surfaces). The true behaviour must lie somewhere in between these extremes.

The results of the analysis of the bedrock movement shows that the effect of the two extreme cases have little impact on the results of the analyses. The difference between the deviator stress and the plastic deformation for the two cases is extremely small according to Figure 7.15 and Figure 7.16.

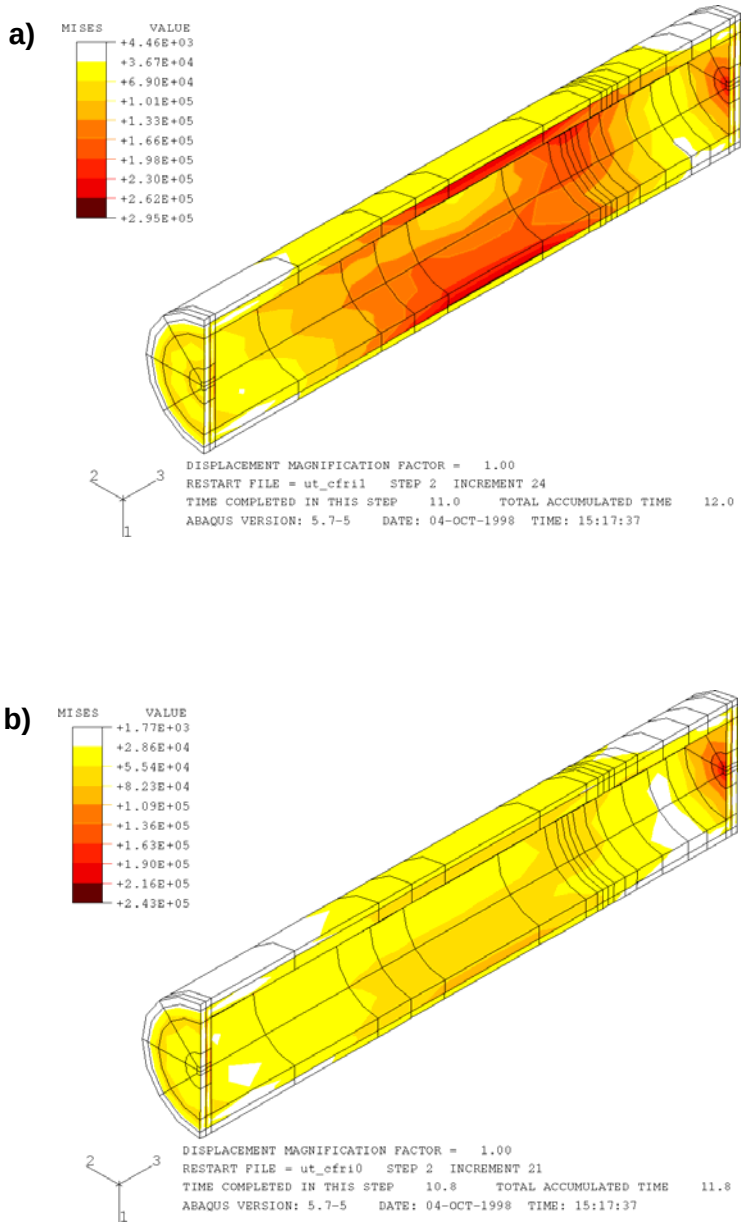


***Figure 7.15*** *Deviator stress in the model for a) full correspondence ($\mu$ = 1), b) slick surfaces ($\mu$ = 0).*

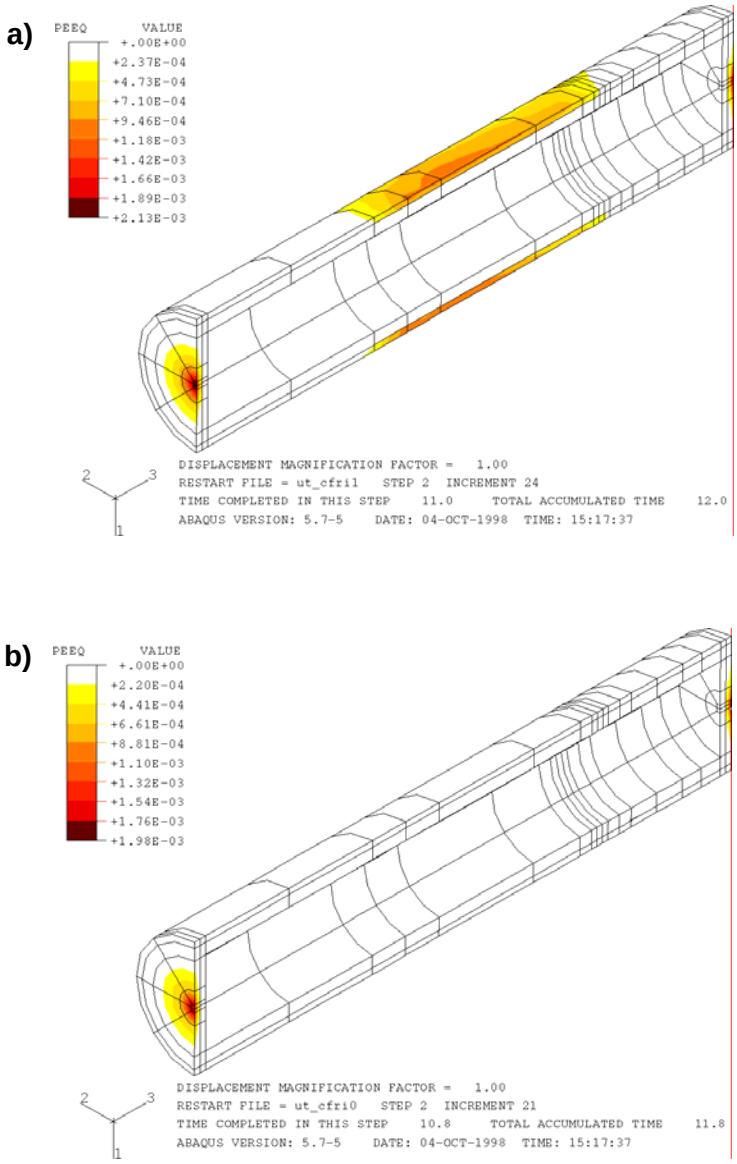


***Figure 7.16*** *Plastic deformations of the model at a) full correspondence ($\mu$ = 1), b) slick surfaces ($\mu$ = 0).*

These analyses illustrate when assuming full interaction in the contact areas, the effect on the canister is assumed. The analysis of the extreme cases furthermore shows that the assumption of full interaction is on the safe side. As a matter of fact the plastic deformations will probably be somewhat smaller for the true model contact properties.

#### 7.2.3.4 Effect of material model for the bentonite

The material properties for the bentonite were determined from laboratory tests according to Drucker-Prager's failure model. Analysis of whether the choice of failure model for the bentonite has any significant impact on the results is interesting as the failure models differ somewhat.

In a first phase the approach was to model the bentonite by "*Critical state*"-parameters and analysing the effect of this. However data for the flow properties of the bentonite

with the"Critical state"-parameters were not available. This is the reason to perform the modeling with Mohr-Coulomb's failure model instead. The correlation between the material properties in the Drucker-Prager's failure model and Mohr-Coulomb model is described in chapter 3.1.

When defining the elastic behaviour in the Mohr-Coulomb failure model ABAQUS uses the modulus of elasticity ($E$) and Poisson's ratio ($\nu$). Analytical determination of the relation between the porous elastic material property ($\kappa$) and the modulus of the elasticity presented some difficulties and poor consistency. An experimental determination of the modulus of elasticity was made to solv these difficulties.

The modulus of elasticity is a linear uniaxial formula between the stresses and strains in the material according to equation (7-1).

$$E = \frac{\sigma_1}{\varepsilon_1} \qquad (7\text{-}1)$$

The material parameter kappa ($\kappa$) describes a non-linear correlation between void ratio and mean effective stress, according to equation (6-1). It is therefore difficult to compare and estimate the correlation between the two parameters. From the analysis with Drucker-Prager model a value of the modulus of elasticity was choosen which gave the same response as $\kappa = 0.21$. This corresponded to a modulus of elasticity of approximately 38 MPa. Earlier calculations for the Na-bentonite MX-80 have been made for a modulus of elasticity of 27 MPa, which in this case gives a somewhat less accurate correspondence.

The analysis of the canister for a movement of the bedrock of 5 cm and the Mohr-Coulomb model gave a stress situation in the model which coincided well with the caes obtained by the Drucker-Prager model. Plastic yield in the canister differed little from each other in the two cases, compare Figure 7.10 and Figure 7.17. However plastic yield in the bentonite was substantially larger for the Mohr-Coulomb model (Figure 7.18), which in turn however does not seem to have any or little effect on the response on the canister. The size of the yield in the bentonite is not very precise, as the value of the modulus of elasticity is very roughly determined. The implication of this is that the size of yield has no influence on the results of the stresses in the canister.

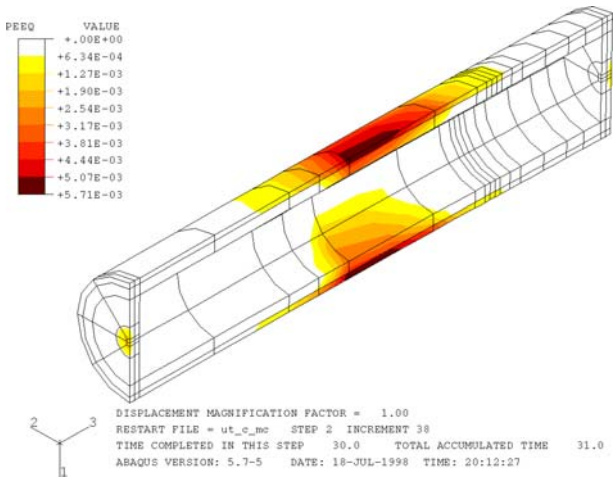


***Figure 7.17*** *Plastic deformation in the canister during shear of the bedrock of 5 cm and modeling of the bentonite with the Mohr-Coulomb yield criteria.*

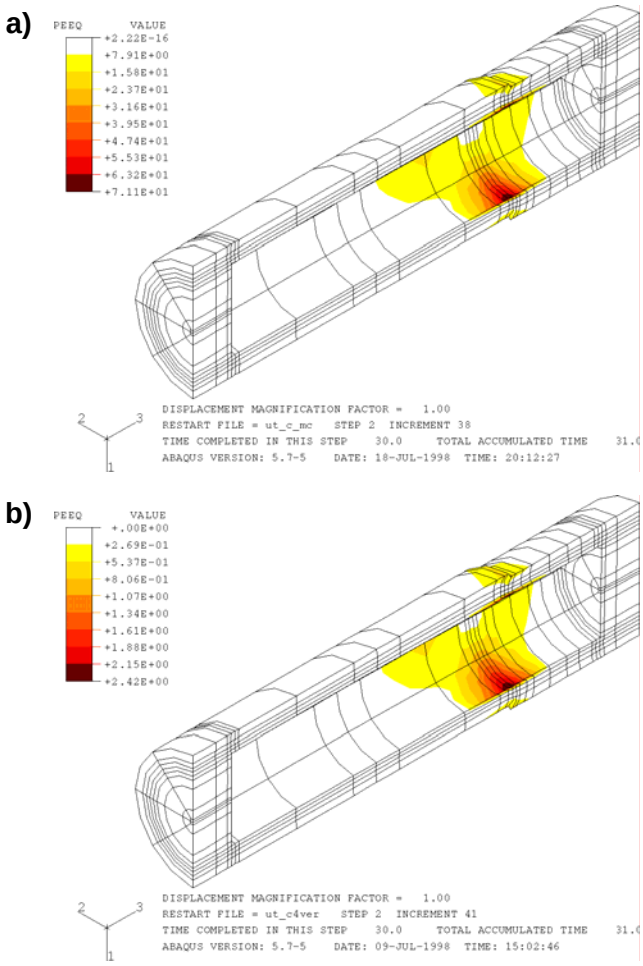


***Figure 7.18*** *Plastic yield of the bentonite at 5 cm shear of the bedrock for the a) Mohr-Coulomb yield model, b) Drucker-Prager yield model.*

### 7.2.3.5 Local swelling

An analysis of the effects of local swelling of the bentonite was performed on the model. In this case the analysis was done with initial state of stress which approximately corresponded to the gravity forces as the bentonite had not started to swell.

The load from local swelling was simplified according to chapter 0 and was analysed for the central section and the end of the canister respectively. The local displacement of the boundary which models the swelling was varied from 5 to 20 cm. A displacement of 20 cm is much compared to the size of the canister. However it was analysed to investigate whether there was a risk for stress concentration or large shear stresses in the canister. Smaller simulations gave a very little effect on the canister. The analysis with a distortion of 20 cm gave a mean effective stress of 300 kPa in the canister and deviator stresses which were of the order of magnitude resulting in no plastic yield in the canister whatsoever according to Figure 7.19.

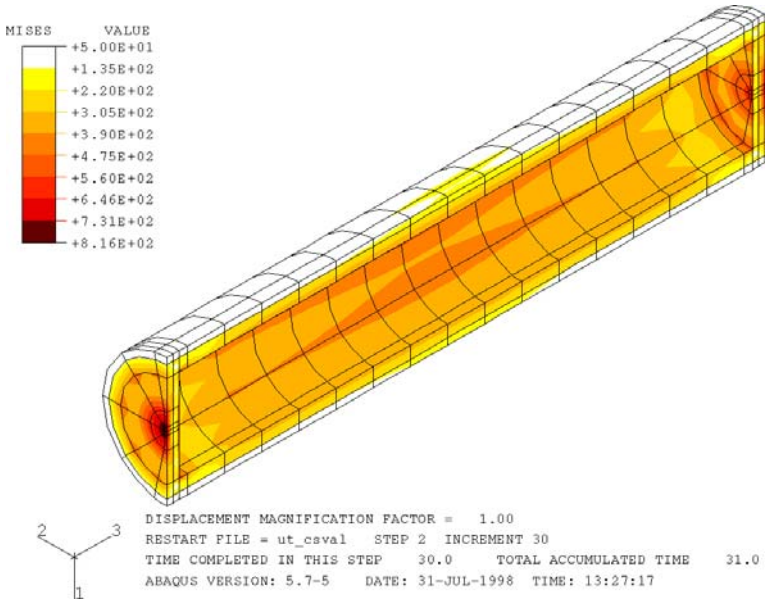


***Figure 7.19*** *Local swelling for the bentonite and resulting deviator stresses in the canister.*

## 7.3 Comments to the analyses

The analyses of the canister show that deformations due to tectonical movements in the bedrock and local swelling respectively will become very small. The size of deformation and possible yielding is affected by the size of the load, which in this case corresponds to the movement of the bedrock. During the analyses of the tectonical movements deformations of 5 and 10 cm were studied. It is important to bear in mind that canisters are placed 500 m down in the bedrock and the place is carefully choosen and investigated concerning fractures and other weaknesses in the surrounding bedrock. From this point of view a local shear of 10 cm can be regarded as a fairly large movement of the bedrock.

In an earlier phase two-dimensional analyses of the canister were performed, see chapter 2. In those investigations the effect of settlement, bearing capacity in the bentonite and different effects of swelling of the bentonite were studied. Those analyses show that settlement and bearing capacity of the bentonite is no threat to the canister whatsoever. Nor does swelling effects in terms of bottom heave or translation of the canister pose any threat. It should be noted that during these analyses three-dimensional effects were disregarded, which in certain respect can be a favourable assumption and in others an unfavourable assumption.

# 8 Conclusions

The analyses performed for the studied canister show, with the made assumptions, that the mechanical strength can be assumed to function as a shield for the nuclear waste from external mechanical factors. The mechanical factors considered are pressures on or movements of the canister developed due to swelling of the bentonite and stresses on the canister caused by 10 cm shear distortion of the bedrock at an unfavorable location.

Preliminary calculations, where assumptions in all aspects have been made on the safe side, show that a number of possible scenarios in the immediate surrounding of the canister will not harm the canister. The scenarios investigated by these preliminary calculations are:

1. Settlement of the canister through the bentonite, so that contact is established with the bedrock
2. Swelling of the bentonite, so that the canister is forced up into the overlaying tunnel
3. Bending of the canister due to local swelling of the bentonite.

Distortion of the bedrock, assumed as a 10 cm lateral movement in the most unfavorable location, resulted in small plastic strains in the copper shell and in the cast iron insert. These plastic strains are, however, so small that the integrity of the canister is not threatened. This is obvious when studying the flow function for the material, which describes the strain hardening properties, i.e. the remaining sheer strength of the material when plastic yield starts. The analyses result in plastic strains in the order of 0.5-1.0 % in the canister. Below, in the yield function for iron and copper are given. The calculated strains are given as a vertical solid line and it can be noted that there is still a long way to failure, roughly 13 % for the iron and 27 % for the copper. This means that further bending of the canister would only result in moderate increase in stresses, while large strains would develop. Further more elaborate analyses is required to determine the necessary shear distortion of the bedrock required to cause failure of the canister. It is possible that shear bands would develop in the bentonite and that the canister would remain intact until the shear distortion of the bedrock corresponds to the total thickness of the bentonite.

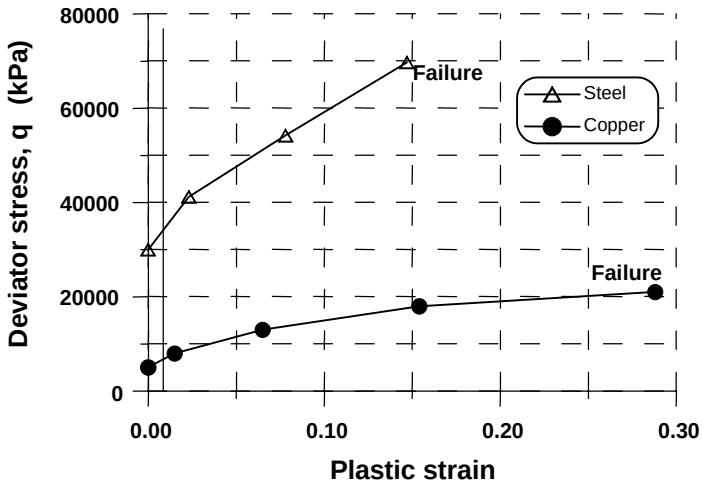


***Figure 8.1*** *Flow function for copper and iron.*

The yield model for the bentonite only marginally effects the response of the stress situation in the canister. However it does show a deviating behavior for the bentonite. For example Mohr-Coulomb's failure model shows in this case a larger plastic yielding in the bentonite compared to Drucker-Prager's yield model. The reliability of these analyses is however questionable as the value of the modulus of elasticity for the bentonite can deviate substantially from those experimentally determined.

Effects of local swelling of the bentonite is not considered as a threat to the canister as it does not result in any deviatoric stresses that create plastic strains in the canister.

The results reported in this report are obtained with realistic assumptions on those material properties that can be fairly well determined and controlled during manufacturing and placing procedure. This relates mainly to geometry and properties of the iron and copper material. The properties of the bedrock and the bentonite can vary over a much wider range and calculations have therefor been carried out for different assumptions, expected as well as extreme conditions.

The bedrock has mostly been modeled as indefinitely stiff and the properties of the bentonite have been varied over a wide range. The results in the report are according to the authors representing worst case scenarios.

The response from the iron insert in the true canister can be simplified and modeled as an equivalent iron insert in the shape of a cylinder with a corresponding bending stiffness. This equivalent iron insert gives a response for the canister, which coincides well with the true iron insert.

Different designs for the canister have also been considered. The results given in this report refer to the design given in section 6.2. Other designs as PWR and BWR have a slightly higher resistance against bending, 32 % and 12 % respectively, which means that the results presented here are on the safe side, if the PWR and BWR should be used.

It should be pointed out that the results presented here all relates to the mechanical properties and static loading of the canister. The transient combined hydro, thermal mechanical properties have not been considered.

# 9 References

**Atkinson, J.H. and Bransby, P.L. (1978):** *The mechanics of soils - an introduction to critical state soil mechanics.* McGraw-Hill, London.

**Börgesson, L. (1990):** *Interim report on the laboratory and theoretical work in modelling the drained and undrained behavior of buffer materials.* SKB Technical Report 90-45.

**Börgesson, L. (1992):** *Interaction between rock, bentonite, buffer and canister. FEM calculations of som mechanical effects on the canister in diffrent disposal concepts.* SKB Technical Report 92-30.

**Börgesson, L., Johannesson, L-E., Sandén, T., and Hernelind, J. (1995):** *Modelling of the physical behaviour of watersaturated clay barriers. Laboratory tests, material models and finit element application.* SKB Technical Report 95-20.

**Chen, W.F. and Mizuno, E. (1990*):** Nonlinear analyzis in soil mechanics. Theory and implementation.* Developments in geotechnical engineering vol. 53. Elsevier, Amsterdam.

**Drucker, D.C. and V. Prager, V., (1952):** *Soil Mechanics and Plastic Analysis or Limit Design*. Quarterly of Applied Mathematics, Vol. 10, No. 2.

**Fang, H.Y. (1991):** *Foundation engineering handbook.* Van Nostrand Reinhold, New York.

**HKS, Hibbit, Karlsson, Sörensen INC. (1997):** ABAQUS/Standard, Theory Manual, User's Manual Volume I, II, III, Post Manual, Version 5.7, HKS, Providence, Rhode Island 02906 USA.

**Powrie, W. (1997):** *Soil Mechanics, Concepts and Applications.* E & FN Spon, an imprint of Chapman and Hall, London.

**Roscoe, K.H. and Burland, J.B. (1968):** *On the generalised stress-strain behaviour of "wet" clay.* Symposium on Engineering Plasticity, Cambridge. Cambridge University Press.

**Roscoe, K.H., Schofield, A.N. and Thurairajah, A. (1963):** *Yielding of clays in states wetter than critical.* Géotechnique 13(3).

**Samuelsson, A. and Wiberg, N-E (1995*):** The finite element method basics.* Institutionen för byggnadsmekanik, Chalmers Tekniska Högskola. Undervisningsskrift 95/96:7.

**Schofield, A.N. and Wroth, C.P. (1968):** *Critical state soil mechanics.* McGraw-Hill, London.

**Vermeer, P.A. (ed), (1995):** *PLAXIS - Finite element code for soil and rock analyzis, User's Manual, Version 6.10, professional version. A.A.* Balkema, Rotterdam.

www.ski.se

**STATENS KÄRNKRAFTINSPEKTION**
Swedish Nuclear Power Inspectorate

**POST/POSTAL ADDRESS** SE-106 58 Stockholm
**BESÖK/OFFICE** Klarabergsviadukten 90
**TELEFON/TELEPHONE** +46 (0)8 698 84 00
**TELEFAX** +46 (0)8 661 90 86
**E-POST/E-MAIL** ski@ski.se
**WEBBPLATS/WEB SITE** www.ski.se